Chilling and forcing temperatures interact to predict the onset of wood formation in Northern Hemisphere conifers

Nicolas Delpierre, Ségolène Lireux, Florian Hartig, Jesus Julio Camarero,
Alissar Cheaïb, Henri Cuny, Annie Deslauriers, Patrick Fonti, Jozica Gricar,
Jian-Guo Huang, et al.

1

2   DR. NICOLAS DELPIERRE (Orcid ID : 0000-0003-0906-9402)

3   DR. JESUS JULIO CAMARERO (Orcid ID : 0000-0003-2436-2922)

4   DR. JIAN-GUO HUANG (Orcid ID : 0000-0003-3830-0415)

5   MS. GUOHUA LIU (Orcid ID : 0000-0003-3164-3829)

6   DR. HARRI MÄKINEN (Orcid ID : 0000-0002-1820-6264)

7   DR. PETER PRISLAN (Orcid ID : 0000-0002-3932-6388)

8

9

11

12

13

14   **Chilling and forcing temperatures interact to predict the onset of wood**

15   **formation in Northern Hemisphere conifers.**

16

17   **Running head**: Temperature dependence of spring xylem onset

18

19   Nicolas Delpierre[1],[*], Ségolène Lireux[1], Florian Hartig[2], J. Julio Camarero[3], Alissar Cheaib[1,4],

20   Katarina Čufar[5], Henri Cuny[6], Annie Deslauriers[7], Patrick Fonti[8], Jožica Gričar[9], Jian-Guo

21   Huang[10], Cornelia Krause[7], Guohua Liu[1,11], Martin de Luis[12], Harri Mäkinen[13], Edurne

22   Martinez del Castillo[12], Hubert Morin[7], Pekka Nöjd[13], Walter Oberhuber[14], Peter Prislan[9],

Sergio Rossi[7,10], Seyedehmasoumeh Saderi[15], Vaclav Treml[16], Hanus Vavrick[17], Cyrille B. K. Rathgeber[15]

[1] Ecologie Systématique Evolution, Univ. Paris-Sud, CNRS, AgroParisTech, Université Paris-Saclay, 91400 Orsay, France

[2] Theoretical Ecology, University of Regensburg, Universitätsstraße 31, 93053 Regensburg, Germany

[3] Instituto Pirenaico de Ecología, CSIC (IPE-CSIC), Avda. Montañana 1005, 50192 Zaragoza, Spain

[4] Département des Sciences de la Vie et de la Terre, Faculté des Sciences – Section IV, Université libanaise Hoch Al Oumara, 1801 Zahlé, Liban

[5] University of Ljubljana, Biotechnical Faculty, Jamnikarjeva 101, SI-1000 Ljubljana, Slovenia

[6] Institut National de l'Information Géographique et Forestière (IGN), 1 rue des blanches terres, 54250 Champigneulles, France

[7] Département des Sciences Fondamentales, Université du Québec à Chicoutimi, 555 boulevard de l'Université, Chicoutimi (QC), Canada

[8] Swiss Federal Research Institute WSL, Zuercherstrasse 111, 8903 Birmensdorf, Switzerland

[9] Slovenian Forestry Institute, Večna pot 2, SI-1000 Ljubljana, Slovenia

[10] Key Laboratory of Vegetation Restoration and Management of Degraded Ecosystems of the Chinese Academy of Sciences, Guangdong Provincial Key Laboratory of Applied Botany, South China Botanical Garden of the Chinese Academy of Sciences, Guangzhou 510650, China

[11] College of Urban and Environmental Sciences, Laboratory for Earth Surface Processes of the Ministry of Education, Peking University, Beijing, China

[12] University of Zaragoza, Department of Geography and Regional Planning, C/Pedro Cerbuna 12, Zaragoza, 50009, Spain

[13] Natural Resources Institute Finland, Tietotie 2, 02150 Espoo, Finland

[14] Department of Botany, University of Innsbruck, 6020 Innsbruck, Austria

[15] Université de Lorraine, AgroParisTech, INRA, Silva, F-54000 Nancy, France

[16] Department of Physical Geography and Geoecology, Faculty of Science, Charles University, Albertov 6, 128 43 Prague, Czech Republic

[17] Department of Wood Science, Faculty of Forestry and Wood Technology, Mendel University in Brno, Zemědělská 3, 613 00 Brno, Czech Republic

54   * author for correspondence : nicolas.delpierre@u-psud.fr ; Tel: 0033+(0)1 69 15 56 77;

55   ORCID : 0000-0003-0906-9402

56

57   **Abstract**

58   The phenology of wood formation is a critical process to consider for predicting how trees

59   from the temperate and boreal zones may react to climate change. Compared to leaf

60   phenology, however, the determinism of wood phenology is still poorly known. Here, we

61   compared for the first time three alternative ecophysiological model classes (*threshold*

62   models, *heat-sum* models and *chilling-influenced heat-sum* models) and an empirical model in

63   their ability to predict the starting date of xylem cell enlargement in spring, for four major

64   Northern Hemisphere conifers (*Larix decidua, Pinus sylvestris*, *Picea abies* and *Picea*

65   *mariana*). We fitted models with Bayesian inference to wood phenological data collected for

66   220 site-years over Europe and Canada. The chilling-influenced heat-sum model received

67   most support for all the four studied species, predicting validation data with a 7.7-day error,

68   which is within one-day of the observed data resolution. We conclude that both chilling and

69   forcing temperatures determine the onset of wood formation in Northern Hemisphere

70   conifers. Importantly, the chilling-influenced heat-sum model showed virtually no spatial bias

71   whichever the species, despite the large environmental gradients considered. This suggests

72   that the spring onset of wood formation is far less affected by local adaptation than by

73   environmentally-driven plasticity. In a context of climate change, we therefore expect rising

74   winter-spring temperature to exert ambivalent effects on the spring onset of wood formation,

75   tending to hasten it through the accumulation of forcing temperature, but imposing a higher

76   forcing-temperature requirement through the lower accumulation of chilling.

77

78   **Keywords**: wood phenology, cambium, phenological models, chilling temperatures, forcing

79   temperatures, conifers.

80   **Introduction**

81   The seasonality of physiological processes is an essential component of terrestrial ecosystem

82   models (TEMs; Delpierre et al., 2012; Kramer, 1995), but is usually poorly represented being

83   mostly confined to the simulation of leaf onset and leaf loss (Delpierre, Vitasse, et al., 2016).

84   In such models, the phenology of non-leaf organs or tissues (e.g. wood) is simulated (i)

85   simultaneous or relative to leaf phenology or (ii) using generic, non-organ-specific

86   temperature functions for modulating the allocation of carbon (Delpierre, Vitasse, et al., 2016

87   ; but see Schiestl-Aalto, Kulmala, Mäkinen, Nikinmaa, & Mäkelä, 2015). This reflects the

88   state of our knowledge on the phenology of trees, which is far more developed for leaves as

89   compared with other organs or tissues (Delpierre, Vitasse, et al., 2016; Ford, Harrington,

90   Bansal, Gould, & St. Clair, 2016). It is difficult to quantify how strongly this knowledge gap

91   affects the predictive ability of TEMs, but it certainly jeopardizes their biological realism

92   (Guillemot et al., 2017). For example, it has been demonstrated in evergreen conifers that the

93   spring resumption of cambium activity generally occurs before budburst (Cuny, Rathgeber,

94   Lebourgeois, Fortin, & Fournier, 2012; Gruber, Strobl, Veit, & Oberhuber, 2010; Huang,

95   Deslauriers, & Rossi, 2014; Michelot, Simard, Rathgeber, Dufrêne, & Damesin, 2012; Rossi

96   et al., 2009). Moreover, several studies have shown that, independent from leaf phenology,

97   the duration of the wood growing season *per se* is a major determinant of wood production

98   (Delpierre, Berveiller, Granda, & Dufrêne, 2016; Lempereur et al., 2015), so that an earlier

99   onset of cambium activity, or a later cessation may result in a higher cell production (Lupi,

100   Morin, Deslauriers, & Rossi, 2010; Mäkinen, Jyske, & Nöjd, 2018). Consequently, there is a

101   clear need for the development of wood phenology modules for inclusion into TEMs.

102   In order to develop wood phenology modules for TEMs, we first have to understand the

103   causal climatic drivers of wood phenology. In the temperate and boreal regions of the

104   Northern Hemisphere, the formation of wood is seasonal and occurs from late spring to early

105   autumn (Rossi et al., 2016, 2008). In spring, cambial mother cells start dividing, producing

106   new derivatives of phloem outward and xylem inward (Larson, 1994; Vaganov, Hughes, &

107   Shashkin, 2006). As a base model for this cycle, several authors have proposed that, just as

108   for buds, the spring resumption of cambium activity is the outcome of a two-phase dormancy

109   period (Begum et al., 2018; Begum, Nakaba, Yamagishi, Oribe, & Funada, 2013; Ford et al.,

110   2016; Little & Bonga, 1974; Rensing & Samuels, 2004). According to this model, cambium

111   activity is prevented by tree's *internal* factors (e.g. physiological state, signals) during the

112   *endo*-dormancy phase; while it resumes during the *eco*-dormancy phase when the *external*

113   conditions are favourable.

114   The main candidate for external conditions driving the resumption of cambium activity in

115   temperate and boreal ecosystems is the spring temperature (as reviewed in Begum et al.,

116   2018; Delpierre, Vitasse, et al., 2016; Larson, 1994). Field observation have shown that spring

117   cambium resumption is usually delayed at high altitudes and latitudes as compared to low

118   altitudes and latitudes (Jyske, Mäkinen, Kalliokoski, & Nöjd, 2014; Moser et al., 2010; Rossi

119   et al., 2016; Rossi, Deslauriers, Anfodillo, & Carraro, 2007; Rossi et al., 2008). Furthermore,

120   local stem heating activated the formation of wood (Gričar et al., 2007), with a gradually

121   increased response to heat applied from winter to spring (Oribe & Kubo, 1997).

122   Based on these evidences, previous studies have developed different model formulations

123   based on spring temperature to predict the timing of cambial resumption. A first model class

124   uses a *temperature threshold* for predicting the onset of cambial activity in conifers from cold

125   biomes (Deslauriers, Rossi, Anfodillo, & Saracino, 2008; Rossi et al., 2007, 2008). However,

126   although this model is able to identify likely periods of cambial activity, its accuracy for

127   predicting the onset of cambial activity from temperature time series is probably low (Fig.

128   S1). Another model class is that of *heat sums* (Giagli, Gricar, Vavrcik, & Gryc, 2016;

129   Schmitt, Jalkanen, & Eckstein, 2004; Seo, Eckstein, Jalkanen, Rickebusch, & Schmitt, 2008;

130   Swidrak, Gruber, Kofler, & Oberhuber, 2011). Their underlying hypothesis is that the

131   cambium resumes its activity (cell division followed by cell differentiation) after sufficient

132   exposure to temperatures above a threshold (so-called *forcing* temperatures). Thus, *heat sum*

133   models mimic the progress of cambium through the eco-dormancy phase, making the implicit

134   hypothesis that the endo- and eco-dormancy phases are sequential, and that endo-dormancy

135   stops at the date when heat accumulation starts (Delpierre, Vitasse, et al., 2016). In practice, a

136   degree-days accumulation is calculated by summing temperatures above a threshold ('base

137   temperature') of typically +5°C (or more rarely lower values e.g. 0-1°C, see Antonucci et al.,

138   2015; Li et al., 2017) from a given day, fixed a priori, before the onset date of cambial

139   reactivation. However, there is no consensus concerning the day or period of year from which

140   the cambium becomes sensitive to *forcing* temperatures. Some studies choose January 1 or

141   spring equinox (Giagli et al., 2016; Schmitt et al., 2004), whereas others (Seo et al., 2008)

142   consider the starting date occurring when trees have experienced a daily mean temperature

143   above +5°C for at least five consecutive days. Moreover, *heat sum* models usually fail in

144   identifying a species-specific heat sum threshold above which cambium would systematically

145   be active (Giagli et al., 2016; Moser et al., 2010), which is indicative of their low structural

146   realism and thus low predictive ability. More recently, *chilling-influenced heat sum* models

147   have been shown able to predict spring cambial reactivation in Douglas fir (Ford et al., 2016).

148   Similar to *heat sum* models, those models were originally designed for describing the progress

149   of primary meristems (i.e. leaf or flower buds) from dormancy to budburst. Their basic

150   hypothesis is that the cambium requires a lower accumulation of *forcing* temperatures during

151   the eco-dormancy phase when exposed to increasing levels of cold temperatures (so-called

152   *chilling* temperatures, (Cannell & Smith, 1983; Little & Bonga, 1974) during the endo-

153   dormancy phase, which may precede or be concomitant to the eco-dormancy phase (Chuine,

154   Garcia de Cortazar-Atauri, Kramer, & Hänninen, 2013). The underlying physiological basis

155   of such *chilling-influenced heat sum* models is not fully understood (Rinne et al., 2001; Singh,

156   Svystun, AlDahmash, Jönsson, & Bhalerao, 2017). Last, a recent study made use of empirical

157   models (linear regression of spring-averaged temperature) to predict the timing of cambial

158   resumption (Rossi et al., 2016).

159   Though previous studies evaluated the ability of the three abovementioned model classes

160   separately in simulating the date of the resumption of cambium activity in spring (threshold-

161   type, Rossi, Morin, Deslauriers, & Plourde, 2011; *heat sums*, Seo et al., 2008; Swidrak et al.,

162   2011; *chilling-influenced heat sums*, Ford et al., 2016; empirical regression, Rossi et al.,

163   2016), there has been no comparison of those models merits on the same dataset. Here, we

164   make use of a large number of field observation data collected over Europe and Canada

165   (GLOBOXYLO database) to conduct for the first time a systematic evaluation of the causal

166   factors affecting the breaking of cambial dormancy, and to propose an improved model of

167   cambial spring resumption. Specifically, by identifying which model structure receives most

168   support from observed data, we aim to evaluate: (1) if the resumption of cambium activity of

169   Northern Hemisphere conifers in spring is more likely caused by the crossing of a given

170   temperature threshold or by an accumulation of heat ("do *threshold* models outperform *heat*

171   *sum* models?") and; (2) if observation data support the existence of a separate endo-dormancy

172   phase that can be broken by chilling exposure ("do *chilling-influenced heat sum* models fit the

173   data best?"). Our hypotheses are (1) *threshold* models are fine for identifying a thermal

174   probability of cambium activity but have low predictive ability since the daily variability of

175   temperature superimposed to seasonal variations cannot serve as a reliable cue for trees; (2)

176   that over large geographical gradients, models incorporating both the effects of chilling and

177   forcing temperature are better able to describe the variability in the beginning of wood

178   formation (since over large climate zones, multiple climate limitations interact). Having

179   identified the model structure best supported by the data, we then evaluate the biological

180   reliability of its inferred parameters, for future use in Terrestrial Ecosystem Models.

181   **Material and methods**

182   **Study sites**

183　The selected study sites were extracted from the GLOBOXYLO database[a], a dataset gathering

184　wood formation and meteorological information collected over the past 15 years from several

185　research teams all over the world. The selected data concern the four most observed

186　coniferous species (*Larix decidua* Mill. (LADE), *Pinus sylvestris* L. (PISY), *Picea abies* L.

187　Karst. (PCAB) and *Picea mariana* (Mill.) BSP (PCMA)), covering a wide range of

188　temperature and photoperiod conditions in the Northern Hemisphere (from 40.0°N to 67.5°N

189　latitude, 79.2°W to 29.4°E longitude, and from 30 m to 2150 m altitudes) (Fig. 1, Table S1).

190　Specifically, the dataset includes wood formation critical dates from 2001 to 2013 over 46

191　study sites for a total of 220 site-years, representing 1105 tree-site-year observations. All

192　sampled trees were dominant individuals. The average (±SD) tree age was 124 ± 70 years,

193　with a diameter at breast height (DBH) of 44 ± 30 cm, and a tree height of 21 ± 8 m (Table

194　S1).

195　**Wood formation data**

196　　　　*Microcore sampling and preparation*

197　At each study site, on average 5±2 trees were chosen and sampled weekly from March-April,

198　depending on local climate conditions, to monitor wood formation. The collection,

199　preparation, and analysis of wood samples followed a common protocol across sites. Wood

200　microcores of 2 mm in diameter and 15-20 mm in length were collected weekly at breast

201　height (1.3±0.3 m) over the growing season, using a Trephor® tool (Rossi, Anfodillo, &

202　Menardi, 2006) or surgical bone sampling needles (Deslauriers, Morin, & Begin, 2003).

203　Microcores were then cut with rotary or sledge microtomes in transverse sections of 10-30 µm

204　thick, stained with safranine and astra blue or cresyl violet acetate and observed under bright-

205　field and polarized light after coloration (Rossi, Deslauriers, & Anfodillo, 2006).

206

207　　　　*Determination of the spring resumption of xylem formation*

208　We focus on the beginning of xylem cell enlargement (bE) as a critical, well-defined marker

209　corresponding to the spring start-up of wood formation. Ultrastructural changes in cambial

210　cells are the very first stage of growth reactivation. The bE occurs somewhat later than the

211　onset of ultrastructural changes in cambial cells; but the latter is very difficult to observe

---

[a] https://www6.nancy.inra.fr/foret-bois-lerfob/Projets/Projets-en-cours/GLOBOXYLO

212   accurately and involves both xylem and phloem cells (Prislan, Čufar, Koch, Schmitt, &

213   Gričar, 2013; Prislan, Schmitt, Koch, Gričar, & Čufar, 2011). It is therefore not often reported

214   in wood formation monitoring studies. To quantify bE, the number of cells in each

215   differentiation zone (cambial, enlargement, thickening, and mature) was counted along at

216   least three radial files on the anatomical sections. Enlarging tracheids were characterized by

217   radial diameter at least twice that of a cambial cell. We defined, at the tree level, the

218   beginning of the enlargement phase (bE) as the date (day of year, DoY) when more than 50%

219   of the observed radial files present at least one first enlarging tracheid (Rathgeber,

220   Longuetaud, Mothe, Cuny, & Le Moguédec, 2011).

Temperature and photoperiod data

222   Mean daily temperatures have been collected at the study sites (Fig. 1). However, local

223   weather stations were usually not installed before the start of the wood formation monitoring.

224   To be able to consider in our models weather conditions also before the monitoring period, we

225   used, for European sites, the WATCH gridded meteorological dataset (grid-resolution $= 0.5°$,

226   Weedon et al., 2014) to extrapolate those missing data, after establishing linear regression

227   between the local and corresponding WATCH temperature data (correlation between

228   overlapping local and WATCH temperature time series was $0.95 < r < 0.99$), and removing

229   the (low) biases of WATCH data. For Canadian sites, i.e. for *Picea mariana*, we did not

230   extrapolate the temperature time series. Day length (the daily duration of the photoperiod)

231   was calculated daily as a function of latitude, using astronomical formulae[b].

Models description

233   We compared three classes of ecophysiological models and one empirical model (Table 1) in

234   their ability to predict the date of onset of xylem cell enlargement phase (bE) in the four tree

235   species of interest. The three model classes are: (i) *threshold* models, (ii) *heat sum* models,

236   (iii) *chilling-influenced heat sum* models. Since the patterns of xylem formation have been

237   strongly related to mean temperatures over large geographical gradients (Rossi et al., 2016),

238   we used an empirical model relating bE to early season (January-June) average temperature as

239   a benchmark for ecophysiological models.

---

[b] See for example Pr Dennis Baldocchi's biometeorology course, lecture number 7
(https://nature.berkeley.edu/biometlab/index.php?scrn=espm129)

240 For all ecophysiological models, we used photoperiod thresholds to delineate the start and end

241 of the endo- and eco-dormancy periods, different to most earlier phenological modelling

242 studies, which usually considered temperature accumulation to start at a given day of year

243 (e.g. usually January 1 in most phenological studies considering *heat sum* models; Linkosalo,

244 Carter, Hakkinen, & Hari, 2000; Seo et al., 2008). This choice was motivated by the fact that

245 our study covers a large latitudinal gradient over which a given calendar day (not perceptible

246 by trees *per se*) may correspond to a large variations in photoperiod (a signal which is

247 perceptible by trees).

248   ***Temperature- and photoperiod-threshold models***

249 In this class of models, we assumed that bE occurs when a given temperature and/or

250 photoperiod threshold has/have been crossed. A first formulation of this model (henceforth

251 referred to as *Tt* model) is:

252 $$bE = \min(d) \ such \ that \ T(d) \geq T^* \ and \ d > -10 \qquad (1)$$

253 where *bE* is the beginning of the xylem enlargement period (DoY), *d* is a day of year (DoY),

254 *T* is the daily average temperature, and *T** is a temperature threshold (°C). We assume that the

255 passing of the temperature threshold necessarily occurs after winter solstice of the previous

256 year (i.e. DoY 355 of the previous year, or DoY -10 of current year).

257 In case *bE* occurs when the thresholds of both temperature and photoperiod have been

258 exceeded, the model (henceforth *TDLt* model) writes:

259 $$\begin{cases} bE = \min(d) \ such \ that \ T(d) \geq T^* \ and \ d > j \\ with \ j = \min(d) \ such \ that \ DL(d) \geq DL^* \ and \ d > -10 \end{cases} \qquad (2)$$

260 where *DL* is the daily photoperiod (hours) and *DL** is a photoperiod-threshold (hours).

261   ***Heat sum model***

262 In the *heat sum* model, we assumed that bE occurs when a given accumulation of heat (above

263 a temperature threshold, i.e. forcing temperatures) has been reached. The model (henceforth

264 *HS* model) takes the form:

265 $$bE = \min(d) \ such \ that \ F(d) \geq F^* \qquad (3)$$

266 $$\text{with } \begin{cases} F(d) = \sum_{F_{start}}^{d} T_{diff}(d) \\ \text{with } T_{diff}(d) = \begin{cases} T(d) - T_f, & \text{if } T \geq T_f \\ 0, & \text{if } T \leq T_f \end{cases} \end{cases} \quad (4)$$

267 where T_f is a temperature-threshold above which forcing temperatures are accumulated, $F(d)$

268 is the heat sum at day d (degree-days) and F^* is the forcing units requirement at which bE

269 occurs (degree-days). In this model, the accumulation of forcing temperature starts at a given

270 photoperiod threshold DL_{Fstart} (hours), occurring after the winter solstice of the previous year

271 such that:

272 $$F_{start} = \min(d) \text{ such that } DL(d) \geq DL_{Fstart} \quad (5)$$

273 $$\text{with } d > -10$$

274 This model simulates the progress of cambium through the eco-dormancy phase and makes

275 the implicit hypothesis that the preceding endo-dormancy phase ends on day F_{start}.

276 ***Chilling-influenced heat sum model***

277 In the chilling-influenced heat sum model (*CiHS* model), the progress of cambium through

278 the endo- and eco-dormancy phases is explicit, and bE occurs at the end of the eco-dormancy

279 phase. During endo-dormancy, cambium division is inhibited by tree internal factors, the

280 effects of which are counteracted by low temperatures. Following the approach proposed by

281 (Cannell & Smith, 1983) for bud meristems, this hypothesis translates into an accumulation of

282 chilling temperatures, quantified as a number of chilling units (C_{tot}, in chill units C.U.). C_{tot} is

283 calculated on a daily basis from C_{start} (DoY), up to the C_{end} date as follows:

284 $$C_{tot}(d) = \sum_{C_{start}}^{C_{end}} R_c(T(d)) \quad (6)$$

285 where the daily rate of chilling (R_c) can be calculated as a linear function of temperature:

286 $$R_c(T(d)) = \begin{cases} 1 \text{ if } T(d) < T_c \\ 0 \text{ if } T(d) \geq T_c \end{cases} \quad (7)$$

287 where T_c is the temperature threshold (°C) below which chilling accumulation occurs.

288 Besides the accumulation of chilling, the model assumes that the progression of the cambium

289 towards bE during eco-dormancy is favoured by the accumulation of forcing temperatures

290 *F(d),* as described in eq. 3-4. The *CiHS* model postulates that, as the accumulation of chilling

291   proceeds, the requirement for forcing temperatures decreases, such that the critical sum of

292   forcing F^* is defined daily, and linearly depends on C_{tot}:

293   $$F^*(d) = g \times C_{tot}(d) + h \quad (8)$$

294   where g is the slope of the relation between required forcing units and chilling-accumulation

295   (degree-days per C.U.), and h is the forcing units requirement in the absence of chilling

296   (degree-days).

297   In this model, both the period of cambium sensitivity to chilling temperatures (delimited by

298   days of year C_{start} and C_{end}, eq. 6) and the start of forcing temperature accumulation (on day

299   of year F_{start}, eq. 4) are parameterized as photoperiods (through parameters DLC_{start}, DLC_{end}

300   and DLF_{start}, respectively; see eq. 5 for the correspondence of e.g. day of year F_{start} with

301   photoperiod DL_{Fstart}). We set the parameter bounds such that DLC_{start} (DLC_{end}) cannot occur

302   earlier than the autumn equinox (winter solstice) of previous year. Letting the model inference

303   procedure free to find the most likely photoperiod limits for chilling and forcing accumulation

304   within a large range (from autumn equinox of the previous year up to summer solstice of the

305   current year), our model may represent several temporal combinations of the chilling and

306   forcing temperature accumulation functions, corresponding to different hypotheses of the

307   interplay between the endo- and eco-dormancy phases (i.e. sequential and parallel; see

308   (Chuine et al., 2013).

309   *Empirical relation with spring average temperature*

310   This empirical model (analogous to Rossi et al., 2016) assumes that bE can be related to

311   spring temperature via a linear regression, such that:

312   $$bE = m_{T_{spg}} \times T_{spg} + p_{T_{spg}}, \quad (9)$$

313   where T_{spg} is the average January-June temperature (°C) calculated for each site-year, and

314   mT_{spg} and pT_{spg} are parameters of the regression line.

315

316   **Parameter estimation and model comparison through Bayesian inference**

317   To assess the models' abilities to simulate bE dates, we randomly split the bE data observed at

318   the tree scale into calibration vs. validation subsets, with 70% of the data for calibration, and

319   30% for validation. We checked that the distribution of the random calibration and validation

320   bE subsets did not differ (Wilcoxon rank sum test, p>0.50). Since the model fitting ability and

321   inferred parameters may depend on the calibration subset used, we repeated the calibration

322   procedure 30 times, using different calibration vs. validation subset combinations. The model

323   evaluation results we report concern validation data, unless indicated.

324   Model parameters were fitted via Bayesian inference (see, e.g. Gelman, Carlin, Stern, &

325   Rubin, 2004, and Fu, Campioli, Van Oijen, Deckmyn, & Janssens, 2012, for application in

326   phenological modelling). The Bayesian framework calculates a posterior estimate and

327   uncertainty for the model parameters, based on a prior distribution and the likelihood, defined

328   as the probability of obtaining the observed data, given the model assumptions with their

329   respective parameters. We use a Gaussian likelihood for all models:

$$330 \qquad L(\theta) = \prod_{i=1,n} \frac{1}{\sigma\sqrt{2\pi}} exp\left[-\frac{1}{2}\left(\frac{P(\theta)_i - O_i}{\sigma}\right)^2\right], \quad \text{(eq. 10)}$$

331   where O_i is the observed bE date (DoY) for site-year-tree i; $P(\theta)_i$ is the bE date (DoY)

332   predicted by the model at point θ in the parameter space, and σ is the standard deviation of

333   the Gaussian distribution.

334   For all models considered, the fitted parameters included temperature and day length

335   thresholds, for which natural extremes are given by the temperature and day length observed

336   across the dataset. We therefore used uniform priors with these values as boundaries.

337   Posterior distributions were estimated with a differential evolution MCMC (DEzs,

338   implemented in the 'BayesianTools' R package, (Hartig, Minnuno, & Paul, 2017)). For each

339   model and species, we ran 200,000 MCMC iterations and confirmed convergence of the chain

340   after burn-in using the Gelman-Rubin criterion (Gelman, Meng, & Stern, 1996), requiring the

341   *psrf* value for all parameters to be smaller than 1.05.

342   As a criterion to compare the models, we used posterior model weights, related to the Bayes

343   factor (BF; Kass & Raftery, 1995, based on the model fit on the validation data. Assuming an

344   equal prior weight on all models, the posterior weight for each model (PMW) is given by:

$$345 \qquad PMW_i = \frac{\text{ML}_i}{\sum_j \text{ML}_j} \qquad \text{(eq. 11)},$$

346   where ML is the marginal likelihood of model i or j. The marginal likelihood is the likelihood

347   of the model for a given dataset, averaged over the parameter uncertainty. In our case, we

348   calculated the ML for the validation data, with parameter uncertainties derived from the

349 posterior estimated with the calibration data. This approach of calculating the ML on a model

350 calibrated by a subset of the data circumvents the known problem of the BF to be highly

351 dependent on parameter priors (see, e.g., O'Hagan, 1995; van Oijen et al., 2013). The PMW

352 can be intuitively interpreted as the probability that the respective model is 'true'. In order to

353 get a representative evaluation of the model abilities, we averaged PMW calculations across

354 the 30 model-validation procedures.

355 Beside PMWs, we calculated for illustration the models' root mean square error of prediction

356 (RMSE) and Akaike Information Criteria (AIC), at the mode of their posterior parameter

357 distributions (MAP).

358 **Quantifying bias in the model predictions**

359 We quantified the bias in model predictions of validation data at the scales of the tree, the

360 site-year, the site ("is the model able to represent the inter-site variability of bE?") and the

361 year ("is the model able to represent the local annual anomaly of bE after removing the local

362 bE average?"). Since there is no consensus in the statistical literature on how to evaluate

363 model bias, we used two different methods. *Method 1*: We plotted and computed the

364 coefficients of the linear ordinary least-squares regression of observed (y-axis) versus

365 predicted (x-axis) data, as recommended by (Piñeiro, Perelman, Guerschman, & Paruelo,

366 2008), and tested the null hypothesis: "the slope of the linear regression equals one and the

367 intercept equals zero" (Wald test) using the LinearHypothesis function from the 'car' R

368 package (Fox & Weisberg, 2011). *Method 2*: we performed a major axis (type II) linear

369 regression of predicted (y-axis) versus observed (x-axis) data, and checked if the 95%-

370 confidence intervals of the slope and intercept included one and zero, respectively (Mesplé,

371 Troussellier, Casellas, & Legendre, 1996).

372

373 **Results**

374 **Wood phenological observations**

375 The observed bE dates spanned 90 days, ranging from March 16 (DoY 75) for a PISY tree at

376 the southernmost site from the database ('Moncayo' site, Spain) to July 2 (DoY 183) for a

377 LADE tree located at 1900-m on an altitudinal gradient ('Lötschental site', Switzerland; Table

378 2). In this dataset, PISY was the earliest species to resume xylem cell enlargement in spring,

379 showing ca. three-week earlier average bE than PCAB and 7-week earlier than PCMA and

380   LADE. The amplitude of bE dates spanned by each species varied from 49 days in PCMA to

381   101 days in PISY, consistent with the size of the climate space occupied by each species in

382   the dataset (Fig. 2).

383

384   **Performance of the models**

385   Whatever the tree species, the chilling-influenced heat sum model (*CiHS*) was identified as

386   the best-supported (most likely) model for predicting bE, displaying the highest posterior

387   model weights over validation data with PMW_{valid} from 0.67 to 1.00 (average 0.90; Table 3).

388   The *CiHS* model largely outperformed models belonging to the *threshold* (i.e. *Tt* and *TDLt*

389   models) or the *heat sum* (*HS*) classes, which both showed nil PMW_{valid} (Table 3). The

390   prediction error of *CiHS* was substantially lower than that of other models structures (e.g.

391   validation RMSE of *CiHS* was on average 1.3 days lower as compared to the heat-sum model

392   *HS*, 3.6 days lower as compared to the temperature-and-photoperiod threshold model (*TDLt*),

393   9.8 days lower as compare to the temperature-threshold model (*Tt*), Table 3). In PCMA, the

394   empirical model predicting bE as a linear function of spring temperature (*MST*) received some

395   support (PMW_{valid}=0.33), but substantially less than *CiHS* (PMW_{valid}=0.67). Beside its

396   performance at the tree scale (Table 3), the *CiHS* model was also good at representing the

397   variability of bE across site-years (Fig. 3), across sites (Suppl. Fig. S2), and across years

398   (Suppl. Fig. S3). The *CiHS* model yielded unbiased predictions of the observations at all

399   aggregation scales according to Method 1 for model bias testing (Table 4). Method 2 pointed

400   more contrasted results: it confirmed the absence of bias at the scales of the site and of the

401   site-year (except for LADE in the latter case; Table 4). However, it pointed biased results at

402   the tree scale, and as regards annual anomalies (except for PCMA). In those cases, Method 2

403   returned that the *CiHS* overestimated early bE and underestimated late bE dates (i.e. slopes of

404   the major axis regression of predicted versus observed dates were less than one).

405   **Posterior parameter estimates for the *CiHS* model**

406   Since the *CiHS* model predicted unknown data best, we looked at its posterior parameter

407   estimates to evaluate their biological reliability. We first note that most parameters of the

408   *CiHS* model could be estimated well (meaning that prior uncertainty was considerably

409   reduced), and that the estimates were similar across the 30 calibration-validation splittings of

410   the data (Fig. 4, see Table S2 for parameter values at the mode of the merged 30 posterior

411   distributions).

412   In all species, chilling accumulation (DL_{Cstart}) started earlier than or close to vernal equinox

413   (corresponding to 12-hour photoperiod, Fig. 4, occurring on DoY 81, Fig. 5) and generally

414   lasted up to late dates (defined by DL_{Cend}), potentially up to the summer solstice when

415   applicable. Notable exceptions were high-latitude PISY and PCAB. In PCAB, the duration of

416   chilling accumulation was very short at high latitudes, virtually non-existent at low latitudes

417   (Fig. 5) and presented a maximum duration of ca. 15 days at intermediate latitudes (ca. 54°N)

418   due to latitudinal variations of the photoperiod course in spring.

419   Chilling accumulation resulted in an actual reduction of the forcing requirement for bE (all g

420   parameters were negative, Fig. 4), with a strong sensitivity to chilling exposure in LADE (-

421   14.9 degree-days / chill unit) and PCAB (-27.9 degree-days / chill unit). The upper

422   temperature threshold for chilling accumulation (T_c) ranged from -5.6°C in PCAB to +6.1°C

423   in PCMA (Fig. 4) with a median across species of +1.6°C. The lower temperature threshold

424   for forcing accumulation (T_f) ranged from -2.9°C in PCAB to +3.4°C in LADE (Fig. 4) with a

425   median across species of +0.15°C. The start of forcing accumulation (defined by DL_{Fstart})

426   looked bounded by vernal equinox (Fig. 5). It occurred later than the start of chilling

427   accumulation in both spruce species (PCAB and PCMA), but earlier than the start of chilling

428   accumulation in PISY and LADE (Fig. 5).

429

430   **Discussion**

431   The purpose of this study was to improve our understanding of the phenology of wood

432   formation, and in particular to unravel the causal triggers for the spring onset of xylem growth

433   in coniferous species. To this end, we evaluated the ability of three families of

434   ecophysiological models and one empirical model to predict the start of the enlargement

435   period of the xylem cells. Our results demonstrate that models based on temperature sums

436   perform better than those based on temperature- and photoperiod-thresholds do (Table 3).

437   Moreover, our results clearly support the chilling-influenced heat sum model (*CiHS*),

438   explicitly considering the processes of chilling and forcing temperature accumulation, for the

439   prediction of the spring onset of wood formation. Beside its high posterior probability

440   compared to the other models, the *CiHS* model also predicted the spring onset of xylem

441 formation with good accuracy. Its RMSE on the validation data, averaging 7.7 days (Table 3),

442 is close to the temporal resolution of micro-core sampling from the trees (i.e. 7 days), and

443 similar to the typical prediction accuracy of budburst (i.e. primary meristems), when deployed

444 over continental gradients (e.g. Basler, 2016). The clear support for a chilling-influenced heat

445 sum for the modelling of spring xylem phenology is different from what is reported in

446 budburst model comparisons. For the latter, heat sums and chilling-influenced heat sums do

447 not usually differ in their fit (Basler, 2016; Vitasse et al., 2011).

448 The identification of the *CiHS* model as receiving most support from the inference procedure

449 suggests that both forcing and chilling temperatures play a role in determining the spring

450 resumption date of xylem formation. To our knowledge, there is no *direct* evidence in the

451 literature of a modulation of the date of onset of xylem cell formation in trees exposed to

452 various chilling temperatures during winter and/or spring. Stem heating experiments showed

453 that an artificial resumption of cambial activity can be triggered during late winter, but not in

454 early winter (Begum, Nakaba, Oribe, Kubo, & Funada, 2010). This observation supports the

455 existence of an endo-dormancy phase, during which the cambium activity is repressed by

456 unknown tree internal factors (Delpierre, Vitasse, et al., 2016, but see Singh et al., 2017, for a

457 review of dormancy processes in primary meristems). However, it does not prove, nor does it

458 quantify the role of chilling temperatures in hastening the reactivation of xylem formation in

459 spring. Thus, there is a clear need for quantifying the actual role of chilling temperatures in

460 modulating the spring resumption of xylem formation, in line with pioneer works regarding

461 buds and seeds (see Sarvas, 1974, reviewed in Hänninen, 2016), which have recently been

462 actualized (e.g. Flynn & Wolkovich, 2018).

463 We delineated the time periods for the accumulation of chilling or forcing temperatures with

464 photoperiod limits, instead of day of year (DoY) as usually done in phenological modelling

465 (see e.g. Olsson and Jönsson, 2014; Basler 2016) for examples over large latitudinal

466 gradients). If the use of DoY is perfectly sound in local studies (i.e. for which the relation

467 between DoY and photoperiod is unequivocal), it is questionable in studies spanning

468 continental scales since plants sense time from variations in the photoperiodic signal. Across a

469 latitudinal gradient, a given photoperiod is reached at different DoYs (except the 12-hour

470 photoperiod occurring at spring equinox (March 20) across the entire gradient). This resulted

471 in large differences in our southern vs. northern study sites as regards the timing of the

472 chilling accumulation for PCAB and the duration of both chilling and forcing accumulation in

473 PISY (Fig. 5), two species spanning large latitudinal gradients in our dataset. Whether such

474 variations of the actual dates of cambium sensitivity to temperatures are realistic remains to

475 be determined. This could experimentally be done by comparing the sensitivity of cambium to

476 chilling in genetically identical plants placed in various photoperiod conditions, either in

477 climate chambers (as done for budburst, e.g. Basler and Körner, 2014) or in natural conditions

478 (e.g. International Phenological Gardens, Chmielewski & Rötzer, 2001).

479 In the *CiHS* model, the threshold temperatures promoting the progress of the eco-dormancy

480 phase (forcing temperature threshold, T_f, ranging from -2.9°C to +3.4°C, Fig. 4) were

481 comparable to values generally used in the modelling of budburst (typically 0°C or +5°C,

482 Hänninen, 2016), based on experimental results (from -5°C to +1°C in, Heide, 1993). On the

483 other hand, the values of threshold chilling temperatures (T_c) determined by the parameter

484 inference procedure span a larger range (from -5.6°C to +6.1°C) and appear quite low in the

485 cases of PCAB (-5.6°C) and LADE (-1.1°C) as compared to the values either determined

486 experimentally in buds and seeds (for which Sarvas, 1974, reports -3°C as a lower limit for

487 chilling effectiveness) or considered by expert judgment (0°C to +4.5°C in Coville, 1920;

488 +2°C to +4°C for cambium in Little & Bonga, 1974) as effective for chilling.

489 From a larger perspective, the questions about the plausibility of parameter values we inferred

490 are further linked with the range of environmental conditions in which the bE data were

491 obtained. Indeed, inferring model parameters from data acquired from trees growing under

492 natural conditions, inevitably exposed to multiple interacting environmental factors (think e.g.

493 of the strong concurrent latitudinal temperature and photoperiod gradient), is not equivalent to

494 inferring them from a controlled experiment where the environmental conditions can be at

495 least partially be disentangled (Verdier et al., 2014), and their biological interpretability is

496 necessarily less generic. However, we noticed that our species-specific parameterizations of

497 the *CiHS* model were able to reproduce the locally observed between-species difference in bE

498 at those sites where two species of interest co-occur (Fig. 6), giving credit to the overall

499 plausibility of the inferred parameters.

500 In this study we used model formulations initially developed for simulating the occurrence of

501 budburst, assuming similar environmental controls of the phenology of primary and

502 secondary meristems (Delpierre, Vitasse, et al., 2016). Even for budburst, those models lack

503 an indisputable biological support (Clark, Salk, Melillo, & Mohan, 2014; Delpierre, Vitasse,

504 et al., 2016). New model formulations for the phenology of budburst appear in the literature

505 from time to time, considering more complex interactions of chilling and forcing temperatures

506 in interaction with photoperiod (e.g. Blümel & Chmielewski, 2012; Caffarra, Donnelly, &

507 Chuine, 2011). Similar to the necessary effort to calibrate and compare those continuous-state

508 budburst models to continuous data (for instance by measuring the release of plasmodesmata

509 closure by callose, which is an indicator of bud endo-dormancy, Singh et al., 2017), a

510 biologically-undisputable modelling of spring cambial activity will require the evaluation of

511 those models with continuous seasonal markers of cambial cells activity (i.e. cytoplasmic

512 changes in cambial cells such as presence and form of microtubules, vacuoles, lipid droplets,

513 plastids and other cell organelles; Begum et al., 2012; Chaffey & Barlow, 2002; Prislan et al.,

514 2013; Rensing & Samuels, 2004), or metabolite content.

515 Even if the *CiHS* model has no clear mechanistic foundation, we remind that the exposure to

516 chilling temperature promotes soluble sugars accumulation from starch conversion, especially

517 sucrose (along with raffinose, stachyose and other metabolites; Sakai & Larcher, 1987;

518 Strimbeck, Schaberg, Fossdal, Schröder, & Kjellsen, 2015) that remain high until spring de-

519 hardening. Since cell production is limited by local sucrose availability (Deslauriers, Huang,

520 Balducci, Beaulieu, & Rossi, 2016), we posit that exposure to chilling temperatures may

521 constitute a local pool of sucrose readily available for cell production when temperatures

522 become favourable for mitosis and/or cell expansion. In case of low chilling, this local

523 sucrose pool would be low, and carbon-fueling for cell formation would rely more on the

524 resumption of photosynthesis, which responds to forcing temperature accumulation (Mäkelä,

525 Hari, Berninger, Hänninen, & Nikinmaa, 2004; Pelkonen & Hari, 1980). This mechanistic

526 hypothesis is coherent with the general behaviour of the *CiHS* model (the required forcing

527 accumulation decreases with increasing chilling exposure), and would explain why we infer in

528 some species low temperature thresholds for chilling accumulation (-1.1°C in LADE, -5.6°C

529 in PCAB). Indeed, the rate of starch to sugar conversion has been shown to be maximum at

530 temperatures from -3°C to -5°C, and continued down to -15°C (in *Salix sachalinensis* twigs,

531 Sakai, 1966).

532 Moreover, the successful use of model structures designed and used to predict budburst to

533 simulate the resumption of cambial spring activity raises the question of the coordination and

534 interaction of the phenologies of tree organs (Delpierre, Vitasse, et al., 2016). Phytohormones

535 can play a significant role; with e.g. auxins produced in expanding buds influencing the rate

536 of stem cambial divisions (see review of Sorce, Giovannelli, Sebastiani, & Anfodillo, 2013).

537 Yet, the important role of auxin is also interconnected with cytokinin in the vascular

538 cambium. Although auxin peak in the middle of cambium and cytokinin in the middle of

539   phloem, the latter acts as a positive regulator of cell division in the vascular cambium by

540   increasing the number of cambial cell (Immanen et al., 2016) because of its crucial role on the

541   cell division cycle (Schaller, Street, & Kieber, 2014). Thus, the resumption of xylem

542   formation in spring is at least partially independent from auxin-producing buds, as clearly

543   demonstrated in stem heating experiments (where xylem formation resumes artificially

544   whereas buds remain dormant, Begum et al., 2010; Gricar et al., 2006; Oribe, Funada, &

545   Kubo, 2003), and from the observed earlier timing of enlargement of new xylem cells, as

546   compared to bud elongation in the evergreen coniferous trees studied here (*Picea abies*, *Pinus*

547   *sylvestris*, *Picea mariana*; Antonucci et al., 2015; Cuny et al., 2012; Huang et al., 2014;

548   Michelot et al., 2012). The presence of auxins in overwintering tissues (Egierszdorff, 1981),

549   and of a local pool of sucrose (see above) may decouple the onset of cambium division and

550   xylem enlargement from the timing of bud elongation, as observed from stem heating

551   experiments; along with the presence of signal-transduction chains involving phytochromes

552   (proteins acting as photoreceptors, i.e. able to sense modifications of the photoperiod) in the

553   cambium (Petterle, Karlberg, & Bhalerao, 2013), this suggests that the cambium may well

554   respond to variations of environmental conditions independently from buds. This hypothesis

555   is supported by inter-annual variability in the delays between the spring phenophases of wood

556   and leaves in both gymnosperms (Cuny et al., 2012) and angiosperms (Takahashi, Okada, &

557   Nobuchi, 2013).

558

559   The chilling-influenced heat sum model produced mostly unbiased results when the data were

560   aggregated at the site-year or at the site scale (Table 4), pointing to its overall accurate

561   capacity of to simulate the spring resumption of xylem formation in coniferous species. Yet,

562   one of our bias-detection methods (method 2) suggested that the model underestimated the

563   range of tree individual bE (in all species, Table 4) and the annual bE anomalies (in 3 out of 4

564   species, Table 4, Fig. S3). Though our models rely on environmental (temperature and

565   photoperiod) data collected at the tree population scale, we conducted the parameter inference

566   with the most basic level of information available (i.e. at the individual tree level, see section

567   2.5). It is clear that part of the model bias that is detected at the individual scale is related to

568   the model structural incapacity to simulate the variety of individual tree responses to the same

569   environment that is observed in a tree population (Delpierre, Guillemot, Dufrêne, Cecchini, &

570   Nicolas, 2017) and can actually be quite large (e.g. the within-population SD of observed bE

571   dates for a given year is 5 days on average, Table 2). Bias in the predictions of annual bE

572   anomalies may further originate from the simplicity of the model structure, which probably

573   does not represent the whole range of environmental interactions resulting in the spring onset

574   of xylem formation.

575   A study aiming at simulating the date of budburst of *Betula pendula* and *Picea abies*

576   individuals from central to Northern Europe (i.e. a bioclimatic scale comparable to the one

577   considered in our work) reported a lower performance over validation data as compared to our

578   results for bE (with prediction RMSE of 8.9 and 9.1 days, respectively for their best heat sum

579   model), along with a non-homogeneous bias over the continent, suggesting a role for the local

580   adaptation of trees phenological traits (Olsson & Jönsson, 2014). It is not clear whether the

581   latitudinal bias observed in Olsson & Jönsson (2014) originates from local adaptation (that

582   has been evidenced several times for budburst, see e.g. Chuine, Mignot, & Belmonte, 2000;

583   Osada et al., 2018; Vitasse, Delzon, Bresson, Michalet, & Kremer, 2009; von Wuehlisch,

584   Krusche, & Muhs, 1995) or is related to the uncertainty of budburst observations recorded

585   through local phenological protocols. The data we use in our work are less prone to such

586   problems since the observations were collected and processed according to a common

587   protocol across the entire study zone (Rathgeber et al., 2011; Rossi et al., 2016). To this

588   respect, we conclude from the absence of bias in the prediction of site average dates of bE

589   (Table 4, Fig. S2) that local adaptation is, if any, of marginal influence in determining bE

590   (Perrin, Rossi, & Isabel, 2017) as compared to the plasticity of bE driven by varying

591   temperature and photoperiod conditions.

592   This study is the first comparative assessment of ecophysiological models aiming at

593   simulating the spring resumption of xylem formation in trees. We demonstrated that chilling-

594   influenced heat sum models are best supported by the data for the four coniferous species

595   studied. Thus, analogous to what is commonly observed for buds, we state that winter-spring

596   temperatures exert ambivalent effects on the spring onset of wood formation (bE) (i.e. on the

597   one hand, warmer temperatures tend to hasten the occurrence of bE through the accumulation

598   of *forcing* temperature, but on the other hand they are associated to less *chilling*, imposing a

599   higher forcing-temperature sum to trigger wood formation). Previous results from (Rossi et

600   al., 2011) suggested that spring warming would result in a continuous trend to earlier bE in

601   the next decades. Our results question these predictions, since warming reduces the number of

602   chilling days. This is probably the cause of the recently evidenced reduced sensitivity of

603   spring leaf phenology to warm temperatures (Fu et al., 2015), which we also forecast to

604   happen for wood formation (note that the length of wood phenology time series is much

605   shorter than for bud phenology, so that this hypothesis remains to be tested).

606   Our work paves the way for the development of ecophysiological models simulating the
607   whole phenological sequence of wood formation. We expect the *CiHS* model to be included
608   as a component of schemes representing the whole seasonal cycle of wood formation, into
609   which subsequent wood formation phases would partially depend on the occurrence of bE
610   (Hänninen & Kramer, 2007; Lupi et al., 2010). Such a model is also urgently needed in
611   ecosystem models of the carbon cycle (Delpierre, Vitasse, et al., 2016) which are undergoing
612   core changes in their representation of wood growth (Guillemot et al., 2017; Schiestl-Aalto et
613   al., 2015).

614

635

636   **Authors' contributions**

637 N.D. and C.B.K.R initiated the project. N.D. designed the study, performed the research and

638 wrote the manuscript. F.H. advised on the Bayesian inference framework. N.D., S.L.,

639 C.B.K.R., F.H. and A.D. analysed results. J.J.C., H.C., K.C., A.D., P.F., J.G., J.-G.H., C.K.,

640 M.L., H.M., E.M.C., P.N., W.O., P.P., S.R., V.T., H.V. and C.B.K.R. collected xylem micro-

641 cores and produced phenological data. C.B.K.R. compiled the phenological database. E.M.C.

642 made Figure 1. All authors commented on the manuscript.

643

644 **References**

645 Antonucci, S., Rossi, S., Deslauriers, A., Lombardi, F., Marchetti, M., & Tognetti, R. (2015). Synchronisms and
646 correlations of spring phenology between apical and lateral meristems in two boreal conifers. *Tree*
647 *Physiology*, *35*(10), 1086–1094. https://doi.org/10.1093/treephys/tpv077

648 Basler, D. (2016). Evaluating phenological models for the prediction of leaf-out dates in six temperate tree
649 species across central Europe. *Agricultural and Forest Meteorology*, *217*, 10–21.
650 https://doi.org/10.1016/j.agrformet.2015.11.007

651 Basler, D., & Körner, C. (2014). Photoperiod and temperature responses of bud swelling and bud burst in four
652 temperate forest tree species. *Tree Physiology*, *34*(4), 377–388. https://doi.org/10.1093/treephys/tpu021

653 Begum, S., Kudo, K., Rahman, M. H., Nakaba, S., Yamagishi, Y., Nabeshima, E., Nugroho, W.D., Oribe, Y.,
654 Kitin, P., Jin, H.-O., & Funada, R. (2018). Climate change and the regulation of wood formation in trees
655 by temperature. *Trees - Structure and Function*, *32*(1), 3–15. https://doi.org/10.1007/s00468-017-1587-6

656 Begum, S., Nakaba, S., Oribe, Y., Kubo, T., & Funada, R. (2010). Cambial sensitivity to rising temperatures by
657 natural condition and artificial heating from late winter to early spring in the evergreen conifer
658 Cryptomeria japonica. *Trees*, *24*(1), 43–52. https://doi.org/10.1007/s00468-009-0377-1

659 Begum, S., Nakaba, S., Yamagishi, Y., Oribe, Y., & Funada, R. (2013). Regulation of cambial activity in
660 relation to environmental conditions: understanding the role of temperature in wood formation of trees.
661 *Physiologia Plantarum*, *147*(1), 46–54. https://doi.org/10.1111/j.1399-3054.2012.01663.x

662 Begum, S., Shibagaki, M., Furusawa, O., Nakaba, S., Yamagishi, Y., Yoshimoto, J., Jin, H.-O., Sano, Y.,
663 Funada, R. (2012). Cold stability of microtubules in wood-forming tissues of conifers during seasons of
664 active and dormant cambium. *Planta*, *235*(1), 165–179. https://doi.org/10.1007/s00425-011-1500-2

665 Blümel, K., & Chmielewski, F. M. (2012). Shortcomings of classical phenological forcing models and a way to
666 overcome them. *Agricultural and Forest Meteorology*, *164*, 10–19.
667 https://doi.org/10.1016/j.agrformet.2012.05.001

668 Caffarra, A., Donnelly, A., & Chuine, I. (2011). Modelling the timing of Betula pubescens budburst. II.
669 Integrating complex effects of photoperiod into process-based models. *Climate Research*, *46*(2), 159–170.
670 https://doi.org/10.3354/cr00983

671   Cannell, M. G. R., & Smith, R. I. (1983). Thermal Time, Chill Days and Prediction of Budburst in Picea
672   sitchensis. *The Journal of Applied Ecology*, *20*(3), 951-963. https://doi.org/10.2307/2403139

673   Chaffey, N., & Barlow, P. (2002). Myosin, microtubules, and microfilaments: Co-operation between cytoskeletal
674   components during cambial cell division and secondary vascular differentiation in trees. *Planta*, *214*(4),
675   526–536. https://doi.org/10.1007/s004250100652

676   Chmielewski, F. M., & Rötzer, T. (2001). Response of tree phenology to climate change across Europe.
677   *Agricultural and Forest Meteorology*, *108*(2), 101–112. https://doi.org/10.1016/S0168-1923(01)00233-7

678   Chuine, I., Garcia de Cortazar-Atauri, I., Kramer, K., & Hänninen, H. (2013). Plant development models. In M.
679   D. Schwartz (Ed.), *Phenology: an integrative environmental science* (2nd ed., pp. 275–293). Dordrecht:
680   Springer.

681   Chuine, I., Mignot, A., & Belmonte, J. (2000). A modelling analysis of the genetic variation of phenology
682   between tree populations. *Journal of Ecology*, *88*, 561–570.

683   Clark, J. S., Salk, C., Melillo, J., & Mohan, J. (2014). Tree phenology responses to winter chilling, spring
684   warming, at north and south range limits. *Functional Ecology*, 28(6), 1344-1355.
685   https://doi.org/10.1111/1365-2435.12309

686   Coville, F. V. (1920). The Influence of Cold in Stimulating the Growth of Plants. *Proceedings of the National
687   Academy of Sciences of the United States of America*, 434–435. https://doi.org/10.1175/1520-
688   0493(1920)48<643b:TIOCIS>2.0.CO;2

689   Cuny, H. E., Rathgeber, C. B. K., Lebourgeois, F., Fortin, M., & Fournier, M. (2012). Life strategies in intra-
690   annual dynamics of wood formation: example of three conifer species in a temperate forest in north-east
691   France. *Tree Physiology*, *32*(5), 612–625. https://doi.org/10.1093/treephys/tps039

692   Delpierre, N., Berveiller, D., Granda, E., & Dufrêne, E. (2016). Wood phenology, not carbon input, controls the
693   interannual variability of wood growth in a temperate oak forest. *New Phytologist*, *210*(2), 459–470.
694   https://doi.org/10.1111/nph.13771

695   Delpierre, N., Guillemot, J., Dufrêne, E., Cecchini, S., & Nicolas, M. (2017). Tree phenological ranks repeat
696   from year to year and correlate with growth in temperate deciduous forests. *Agricultural and Forest
697   Meteorology*, *234–235*, 1–10. https://doi.org/10.1016/j.agrformet.2016.12.008

698   Delpierre, N., Soudani, K., François, C., Le Maire, G., Bernhofer, C., Kutsch, W., Misson, L., Rambal, S.,
699   Vesala, T., & Dufrêne, E. (2012). Quantifying the influence of climate and biological drivers on the
700   interannual variability of carbon exchanges in European forests through process-based modelling.
701   *Agricultural and Forest Meteorology*, *154–155*, 99–112. https://doi.org/10.1016/j.agrformet.2011.10.010

702   Delpierre, N., Vitasse, Y., Chuine, I., Guillemot, J., Bazot, S., Rutishauser, T., & Rathgeber, C. B. K. (2016).
703   Temperate and boreal forest tree phenology: from organ-scale processes to terrestrial ecosystem models.
704   *Annals of Forest Science*, *73*(1), 5–25. https://doi.org/10.1007/s13595-015-0477-6

705   Deslauriers, A., Huang, J.-G., Balducci, L., Beaulieu, M., & Rossi, S. (2016). The Contribution of Carbon and
706   Water in Modulating Wood Formation in Black Spruce Saplings. *Plant Physiology*, *170*(4), 2072–2084.
707   https://doi.org/10.1104/pp.15.01525

708   Deslauriers, A., Morin, H., & Begin, Y. (2003). Cellular phenology of annual ring formation of Abies balsamea
709   in the Quebec boreal forest (Canada). *Canadian Journal of Forest Research*, *33*(2), 190–200.
710   https://doi.org/10.1139/x02-178

711   Deslauriers, A., Rossi, S., Anfodillo, T., & Saracino, A. (2008). Cambial phenology, wood formation and
712   temperature thresholds in two contrasting years at high altitude in southern Italy. *Tree Physiology*.
713   https://doi.org/10.1093/treephys/28.6.863

714   Egierszdorff, S. (1981). The role of auxin stored in scots pine trunk during spring activation of cambial activity.
715   *Biologia Plantarum*, *23*(2), 110–115. https://doi.org/10.1007/BF02878415

716   Flynn, D. F. B., & Wolkovich, E. M. (2018). Temperature and photoperiod drive spring phenology across all
717   species in a temperate forest community. *New Phytologist*. https://doi.org/10.1111/nph.15232

718   Ford, K. R., Harrington, C. A., Bansal, S., Gould, P. J., & St. Clair, J. B. (2016). Will changes in phenology track
719   climate change? A study of growth initiation timing in coast Douglas-fir. *Global Change Biology*, *22*(11),
720   3712–3723. https://doi.org/10.1111/gcb.13328

721   Fox, J., & Weisberg, S. (2011). *An R companion to applied regression. SAGE.*
722   https://doi.org/10.1177/0049124105277200

723   Fu, Y. H., Campioli, M., Van Oijen, M., Deckmyn, G., & Janssens, I. A. (2012). Bayesian comparison of six
724   different temperature-based budburst models for four temperate tree species. *Ecological Modelling*, *230*,
725   92–100. https://doi.org/10.1016/j.ecolmodel.2012.01.010

726   Fu, Y. H., Zhao, H., Piao, S., Peaucelle, M., Peng, S., Zhou, G., Ciais, P., Huang, M., Menzel, A., Peñuelas, J.,
727   Song, Y., Vitasse, Y., Zeng, Z., & Janssens, I. A. (2015). Declining global warming effects on the
728   phenology of spring leaf unfolding. *Nature*, *526*(7571), 104–107. https://doi.org/10.1038/nature15402

729   Gelman, A., Carlin, J. B., Stern, H. S., & Rubin, D. B. (2004). *Bayesian Data Analysis. Chapman Texts in*
730   *Statistical Science Series*. https://doi.org/10.1007/s13398-014-0173-7.2

731   Gelman, A., Meng, X.-L., & Stern, H. (1996). Posterior predictive assessment of model fitness via realized
732   discrepancies. *Statistica Sinica*, *6*(4), 733–807. https://doi.org/10.1.1.142.9951

733   Giagli, K., Gricar, J., Vavrcik, H., & Gryc, V. (2016). Nine-year monitoring of cambial seasonality and cell
734   production in Norway spruce, *9*, 375–382. https://doi.org/10.3832/ifor1771-008

735   Gričar, J., Zupančič, M., Čufar, K., Koch, G., Schmitt, U., & Oven, P. (2006). Effect of local heating and cooling
736   on cambial activity and cell differentiation in the stem of Norway spruce (Picea abies). *Annals of Botany*,
737   *97*(6), 943–951. https://doi.org/10.1093/aob/mcl050

738 Gričar, J., Zupančič, M., Čufar, K., & Oven, P. (2007). Regular cambial activity and xylem and phloem
739   formation in locally heated and cooled stem portions of Norway spruce. *Wood Science and Technology*,
740   *41*(6), 463–475. https://doi.org/10.1007/s00226-006-0109-2

741 Gruber, A., Strobl, S., Veit, B., & Oberhuber, W. (2010). Impact of drought on the temporal dynamics of wood
742   formation in Pinus sylvestris. *Tree Physiology*, *30*(4), 490–501. https://doi.org/10.1093/treephys/tpq003

743 Guillemot, J., Francois, C., Hmimina, G., Dufrêne, E., Martin-StPaul, N. K., Soudani, K., Marie, G., Ourcival,
744   J.-M., & Delpierre, N. (2017). Environmental control of carbon allocation matters for modelling forest
745   growth. *New Phytologist*, *214*(1). https://doi.org/10.1111/nph.14320

746 Hänninen, H. (2016). *Boreal and Temperate Trees in a Changing Climate*. Dordrecht: Springer Netherlands.
747   https://doi.org/10.1007/978-94-017-7549-6

748 Hänninen, H., & Kramer, K. (2007). A Framework for Modelling the Annual Cycle of Trees in Boreal and
749   Temperate. *Silva Fennica*, *41*(1), 167–205.

750 Hartig, F., Minnuno, F., & Paul, S. (2017). BayesianTools: General-Purpose MCMC and SMC Samplers and
751   Tools for Bayesian Statistics. R package version 0.1.5.

752 Heide, O. (1993). Daylength and thermal time responses of budburst during dormancy release in some northern
753   deciduous trees. *Physiologia Plantarum*, *88*(4), 531–540. Retrieved from
754   http://onlinelibrary.wiley.com/doi/10.1111/j.1399-3054.1993.tb01368.x/abstract

755 Huang, J.-G., Deslauriers, A., & Rossi, S. (2014). Xylem formation can be modeled statistically as a function of
756   primary growth and cambium activity. *The New Phytologist*, *203*(3), 831–841.
757   https://doi.org/10.1111/nph.12859

758 Immanen, J., Nieminen, K., Smolander, O. P., Kojima, M., Alonso Serra, J., Koskinen, P., Zhang, J., Elo, A.,
759   Mähönen, A. P., Street, N., Bhalerao, R. P., Paulin, L., Auvinen, P., Sakakibara, H., & Helariutta, Y.
760   (2016). Cytokinin and Auxin Display Distinct but Interconnected Distribution and Signaling Profiles to
761   Stimulate Cambial Activity. *Current Biology*, *26*(15), 1990–1997.
762   https://doi.org/10.1016/j.cub.2016.05.053

763 Jyske, T., Mäkinen, H., Kalliokoski, T., & Nöjd, P. (2014). Intra-annual tracheid production of Norway spruce
764   and Scots pine across a latitudinal gradient in Finland. *Agricultural and Forest Meteorology*, *194*, 241–
765   254. https://doi.org/10.1016/j.agrformet.2014.04.015

766 Kass, R. E., & Raftery, A. E. (1995). Bayes factors. *Journal of the American Statistical Association*, *90*(430),
767   773–795. https://doi.org/10.1080/01621459.1995.10476572

768 Kramer, K. (1995). Modelling comparison to evaluate the importance of phenology for the effects of climate
769   change on growth of temperate-zone deciduous trees. *Climate Research*, *5*, 119–130.

770 Larson, P. (1994). *The vascular cambium: development and structure. Springer*. https://doi.org/10.1007/978-3-

642-78466-8

Lempereur, M., Martin-stpaul, N. K., Damesin, C., Joffre, R., Ourcival, J., Rocheteau, A., & Rambal, S. (2015). Growth duration is a better predictor of stem increment than carbon supply in a Mediterranean oak forest : implications for assessing forest productivity under climate change. *New Phytologist*, *207*, 579–590.

Li, X., Liang, E., Gričar, J., Rossi, S., Čufar, K., & Ellison, A. M. (2017). Critical minimum temperature limits xylogenesis and maintains treelines on the southeastern Tibetan Plateau. *Science Bulletin*, *62*(11), 804–812. https://doi.org/10.1016/j.scib.2017.04.025

Linkosalo, T., Carter, T. R., Hakkinen, R., & Hari, P. (2000). Predicting spring phenology and frost damage risk of Betula spp. under climatic warming: A comparison of two models. *Tree Physiology*, *20*(17), 1175–1182. https://doi.org/10.1093/treephys/20.17.1175

Little, C. H. A., & Bonga, J. M. (1974). Rest in the cambium of Abies balsamea. *Canadian Journal of Botany*, *52*, 1723–1730.

Lupi, C., Morin, H., Deslauriers, A., & Rossi, S. (2010). Xylem phenology and wood production: resolving the chicken-or-egg dilemma. *Plant, Cell & Environment*, *33*(10), 1721–1730. https://doi.org/10.1111/j.1365-3040.2010.02176.x

Mäkelä, A., Hari, P., Berninger, F., Hänninen, H., & Nikinmaa, E. (2004). Acclimation of photosynthetic capacity in Scots pine to the annual cycle of temperature. *Tree Physiology*, *24*(4), 369–376. https://doi.org/10.1093/treephys/24.4.369

Mäkinen, H., Jyske, T., & Nöjd, P. (2018). Dynamics of diameter and height increment of Norway spruce and Scots pine in southern Finland. *Annals of Forest Science*, *75*(1): 28. https://doi.org/10.1007/s13595-018-0710-1

Mesplé, F., Troussellier, M., Casellas, C., & Legendre, P. (1996). Evaluation of simple statistical criteria to qualify a simulation. *Ecological Modelling, 88*, 9-18. https://doi.org/10.1016/0304-3800(95)00033-X

Michelot, A., Simard, S., Rathgeber, C., Dufrêne, E., & Damesin, C. (2012). Comparing the intra-annual wood formation of three European species (Fagus sylvatica, Quercus petraea and Pinus sylvestris) as related to leaf phenology and non-structural carbohydrate dynamics. *Tree Physiology*, *32*(8), 1033–1045. https://doi.org/10.1093/treephys/tps052

Moser, L., Fonti, P., Büntgen, U., Esper, J., Luterbacher, J., Franzen, J., & Frank, D. (2010). Timing and duration of European larch growing season along altitudinal gradients in the Swiss Alps. *Tree Physiology*, *30*(2), 225–233. https://doi.org/10.1093/treephys/tpp108

O'Hagan, A. (1995). Fractional Bayes Factors for Model Comparison. *Journal of the Royal Statistical Society: Series B (Methodological)*, *57*(1), 99–138. https://doi.org/10.2307/2346088

Olsson, C., & Jönsson, A. M. (2014). Process-based models not always better than empirical models for

804   simulating budburst of Norway spruce and birch in Europe. *Global Change Biology*, *20*(11), 3492–3507.
805   https://doi.org/10.1111/gcb.12593

806 Oribe, Y., Funada, R., & Kubo, T. (2003). Relationships between cambial activity , cell differentiation and the
807   localization of starch in storage tissues around the cambium in locally heated stems of Abies sachalinensis
808   (Schmidt) Masters. *Trees*, *17*, 185–192. https://doi.org/10.1007/s00468-002-0231-1

809 Oribe, Y., & Kubo, T. (1997). Effect of heat on cambial reactivation during winter dormancy in evergreen and
810   deciduous conifers. *Tree Physiology*, *17*(2), 81–87. https://doi.org/10.1093/treephys/17.2.81

811 Osada, N., Murase, K., Tsuji, K., Sawada, H., Nunokawa, K., Tsukahara, M., & Hiura, T. (2018). Genetic
812   differentiation in the timing of budburst in Fagus crenata in relation to temperature and photoperiod.
813   *International Journal of Biometeorology*, 1–14. https://doi.org/10.1007/s00484-018-1579-2

814 Pelkonen, P., & Hari, P. (1980). The dependence of the springtime recovery of CO_2 uptake in Scots pine on
815   temperature and internal factors. *Flora*, *169*, 398–404. Retrieved from citeulike-article-id:7556840

816 Perrin, M., Rossi, S., & Isabel, N. (2017). Synchronisms between bud and cambium phenology in black spruce:
817   Early-flushing provenances exhibit early xylem formation. *Tree Physiology*, *37*(5), 593–603.
818   https://doi.org/10.1093/treephys/tpx019

819 Petterle, A., Karlberg, A., & Bhalerao, R. P. (2013). Daylength mediated control of seasonal growth patterns in
820   perennial trees. *Current Opinion in Plant Biology*. https://doi.org/10.1016/j.pbi.2013.02.006

821 Piñeiro, G., Perelman, S., Guerschman, J. P., & Paruelo, J. M. (2008). How to evaluate models: Observed vs.
822   predicted or predicted vs. observed? *Ecological Modelling*, *216*(3–4), 316–322.
823   https://doi.org/10.1016/j.ecolmodel.2008.05.006

824 Prislan, P., Čufar, K., Koch, G., Schmitt, U., & Gričar, J. (2013). Review of cellular and subcellular changes in
825   the cambium. *IAWA Journal*, *34*(4), 391–407. https://doi.org/10.1163/22941932-00000032

826 Prislan, P., Schmitt, U., Koch, G., Gričar, J., & Čufar, K. (2011). Seasonal ultrastructural changes in the cambial
827   zone of beech (Fagus Sylvatica) grown at two different altitudes. *IAWA Journal*, *32*(4), 443–459.

828 Rathgeber, C. B. K., Longuetaud, F., Mothe, F., Cuny, H., & Le Moguédec, G. (2011). Phenology of wood
829   formation: Data processing, analysis and visualisation using R (package CAVIAR). *Dendrochronologia*,
830   *29*(3), 139–149. https://doi.org/10.1016/j.dendro.2011.01.004

831 Rensing, K. H., & Samuels, a. L. (2004). Cellular changes associated with rest and quiescence in winter-
832   dormant vascular cambium of Pinus contorta. *Trees*, *18*(4), 373–380. https://doi.org/10.1007/s00468-003-
833   0314-7

834 Rinne, P. L. H., Kaikuranta, P. M., Van Der Schoot, C., Schoot, C. Van Der, Conservation, N., & Physiology, P.
835   D. (2001). The shoot apical meristem restores its symplasmic organization during chilling-induced release
836   from dormancy. *The Plant Journal*, *26*(3), 249–264. https://doi.org/10.1046/j.1365-313X.2001.01022.x

837 Rossi, S., Anfodillo, T., Čufar, K., Cuny, H. E., Deslauriers, A., Fonti, P., Frank, D., Gričar, J., Gruber, A.,
838   Huang, J.-G., Jyske, T., Kaspar, J., King, G., Krause, C., Liang, E., Mäkinen, H., Morin, H., Nöjd, P.,
839   Oberhuber, W., Prislan, P., Rathgeber, C.B.K., Saracino, A., Swidrak, I., & Treml, V. (2016). Pattern of
840   xylem phenology in conifers of cold ecosystems at the Northern Hemisphere. *Global Change Biology*,
841   *22*(11), 3804–3813. https://doi.org/10.1111/gcb.13317

842 Rossi, S., Anfodillo, T., & Menardi, R. (2006). TREPHOR: a new tool for sampling microcores from tree stems.
843   *IAWA Journal*, *27*(1), 89–97.

844 Rossi, S., Deslauriers, A., & Anfodillo, T. (2006). Assessment of cambial activity and xylogenesis by
845   microsampling tree species: An example at the Alpine timberline. *IAWA Journal*.
846   https://doi.org/10.1163/22941932-90000161

847 Rossi, S., Deslauriers, A., Anfodillo, T., & Carraro, V. (2007). Evidence of threshold temperatures for
848   xylogenesis in conifers at high altitudes. *Oecologia*, *152*(1), 1–12. https://doi.org/10.1007/s00442-006-
849   0625-7

850 Rossi, S., Deslauriers, A., Griçar, J., Seo, J.-W., Rathgeber, C. B. K., Anfodillo, T., Morin, H., Levanic, T.,
851   Oven, P., & Jalkanen, R. (2008). Critical temperatures for xylogenesis in conifers of cold climates. *Global
852   Ecology and Biogeography*, *17*(6), 696–707. https://doi.org/10.1111/j.1466-8238.2008.00417.x

853 Rossi, S., Morin, H., Deslauriers, A., & Plourde, P.-Y. (2011). Predicting xylem phenology in black spruce under
854   climate warming. *Global Change Biology*, *17*(1), 614–625. https://doi.org/10.1111/j.1365-
855   2486.2010.02191.x

856 Rossi, S., Rathgeber, C. B. K., Deslauriers, A., Sergio, R., Cyrille, B. K. R., & Annie, D. (2009). Comparing
857   needle and shoot phenology with xylem development on three conifer species in Italy. *Annals of Forest
858   Science*, *66*(2), 1–8.

859 Sakai, A. (1966). Studies of Frost Hardiness in Woody Plants. II. Effect of Temperature on Hardening. *Plant
860   Physiology*, *41*(2), 353–359. https://doi.org/10.1104/pp.41.2.353

861 Sakai, A., & Larcher, W. (1987). *Frost survival of plants: responses and adaptation to freezing stress*.
862   *Ecological studies*. https://doi.org/10.1007/BF02854542

863 Sarvas, R. (1974). *Investigations on the annual cycle of development of forest trees. II. Autumn dormancy and
864   winter dormancy. Communicationes Instituti Forestalis Fenniae*.

865 Schaller, G. E., Street, I. H., & Kieber, J. J. (2014). Cytokinin and the cell cycle. *Current Opinion in Plant
866   Biology*, *21*, 7–15. https://doi.org/10.1016/j.pbi.2014.05.015

867 Schiestl-Aalto, P., Kulmala, L., Mäkinen, H., Nikinmaa, E., & Mäkelä, A. (2015). CASSIA - a dynamic model
868   for predicting intra-annual sink demand and interannual growth variation in Scots pine. *New Phytologist*,
869   *206*(2), 647–659. https://doi.org/10.1111/nph.13275

870 Schmitt, U., Jalkanen, R., & Eckstein, D. (2004). Cambium dynamics of Pinus sylvestris and Betula spp. in the
871   northern boreal forest in Finland. *Silva Fennica*, *38*(2), 167–178. https://doi.org/10.14214/sf.426

872 Seo, J.-W. J., Eckstein, D., Jalkanen, R., Rickebusch, S., & Schmitt, U. W. E. (2008). Estimating the onset of
873   cambial activity in Scots pine in northern Finland by means of the heat-sum approach. *Tree Physiology*,
874   *28*(1), 105–112. https://doi.org/10.1093/treephys/28.1.105

875 Singh, R. K., Svystun, T., AlDahmash, B., Jönsson, A. M., & Bhalerao, R. P. (2017). Photoperiod- and
876   temperature-mediated control of phenology in trees – a molecular perspective. *New Phytologist*.
877   https://doi.org/10.1111/nph.14346

878 Sorce, C., Giovannelli, A., Sebastiani, L., & Anfodillo, T. (2013). Hormonal signals involved in the regulation of
879   cambial activity, xylogenesis and vessel patterning in trees. *Plant Cell Reports*, *32*(6), 885–898.
880   https://doi.org/10.1007/s00299-013-1431-4

881 Strimbeck, G. R., Schaberg, P. G., Fossdal, C. G., Schröder, W. P., & Kjellsen, T. D. (2015). Extreme low
882   temperature tolerance in woody plants. *Frontiers in Plant Science*, *6,* 884.
883   https://doi.org/10.3389/fpls.2015.00884

884 Swidrak, I., Gruber, A., Kofler, W., & Oberhuber, W. (2011). Effects of environmental conditions on onset of
885   xylem growth in Pinus sylvestris under drought. *Tree Physiology*, *31*(5), 483–493.
886   https://doi.org/10.1093/treephys/tpr034

887 Takahashi, S., Okada, N., & Nobuchi, T. (2013). Relationship between the timing of vessel formation and leaf
888   phenology in ten ring-porous and diffuse-porous deciduous tree species. *Ecological Research*, *28*(4), 615–
889   624. https://doi.org/10.1007/s11284-013-1053-x

890 Vaganov, E. A., Hughes, M. K., & Shashkin, A. V. (2006). *Growth Dynamics of Conifer Tree Rings: Images of*
891   *Past and Future Environments . Springer* (Vol. 83). https://doi.org/10.1007/3-540-31298-6

892 van Oijen, M., Reyer, C., Bohn, F. J., Cameron, D. R., Deckmyn, G., Flechsig, M., Härkönen, S., Hartig., F.,
893   Huth, A., Kiviste, A., Lasch, P., Mäkelä, A., Mette, T., Minnuno, F., & Rammer, W. (2013). Bayesian
894   calibration, comparison and averaging of six forest models, using data from Scots pine stands across
895   Europe. *Forest Ecology and Management*, *289*, 255–268. https://doi.org/10.1016/j.foreco.2012.09.043

896 Verdier, B., Jouanneau, I., Simonnet, B., Rabin, C., Van Dooren, T. J. M., Delpierre, N., Clobert, J., Abbadie, L.,
897   Ferrière, R., & Le Galliard, J. F. (2014). Climate and atmosphere simulator for experiments on ecological
898   systems in changing environments. *Environmental Science and Technology*, *48*(15), 8744–8753.
899   https://doi.org/10.1021/es405467s

900 Vitasse, Y., Delzon, S., Bresson, C. C., Michalet, R., & Kremer, A. (2009). Altitudinal differentiation in growth
901   and phenology among populations of temperate-zone tree species growing in a common garden. *Canadian*
902   *Journal of Forest Research*, *39*(7), 1259–1269. https://doi.org/10.1139/X09-054

903 Vitasse, Y., François, C., Delpierre, N., Dufrêne, E., Kremer, A., Chuine, I., & Delzon, S. (2011). Assessing the

904   effects of climate change on the phenology of European temperate trees. *Agricultural and Forest*

905   *Meteorology*, *151*(7), 969–980. https://doi.org/10.1016/j.agrformet.2011.03.003

906   von Wuehlisch, G., Krusche, D., & Muhs, H. J. (1995). Variation in temperature sum requirement for flushing of

907   beech provenances. *Silvae Genetica*, *44 (5-6),* 343-346.

908   Weedon, G. P., Balsamo, G., Bellouin, N., Gomes, S., Best, M. J., & Viterbo, P. (2014). The WFDEI

909   meteorological forcing data set: WATCH Forcing Data methodology applied to ERA-Interim reanalysis

910   data. *Water Resources Research*, *50*(9), 7505–7514. https://doi.org/10.1002/2014WR015638

911

912   **Tables**

913   **Table 1. Overview of the tested models and their parameters**. T_a= daily average air

914   temperature (°C); *DL*= photoperiod (hours). See text for definition of the model parameters.

Model name	Type	Environmental variables	Fitted parameters (number)	Equation reference
Tt	temperature *threshold*	T_a	T* (1)	1
TDLt	temperature and photoperiod *thresholds*	T_a, DL	DL*, T* (2)	2
HS	*Heat sum*	T_a, DL	DLF_{start}, T_f, F* (3)	3-5
CiHS	*Chilling-influenced heat sum*	T_a, DL	DLC_{start}, DLC_{end}, DLF_{start}, T_c, T_f, g, h (7)	6-8
MST	Regression line	January-June average temperature	mT_{spg}, pT_{spg} (2)	9

915

916 **Table 2. Overview of the wood phenology data**. bE= date of the beginning of xylem cell

917 enlargement (DoY), ΔbE= amplitude of bE dates (days). The 'within site-year SD' metric is

918 the average standard deviation of bE among trees sampled on a given site-year.

Tree species	Number of site-years	Number of observations	Mean bE (DoY)	SD of bE (days)	Min. bE (DoY)	Max. bE (DoY)	ΔbE within-species (days)	Within-site-year SD (days)
LADE	62	300	150	12	118	183	65	5.4
PISY	37	175	112	20	75	176	101	5.4
PCAB	77	336	136	16	101	177	76	4.2
PCMA	42	294	152	9	128	177	49	4.8

919 **Table 3. Model performance comparison**. PMW= posterior model weight (eq. 11); RMSE= root mean square error (days); ΔAICc=

920 differential Akaike Information Criterion, corrected for small sample biases (calculated as the difference from minimum AICc across all models;

921 according to this metric, the best model at maximum likelihood has a score of 0). PMWs are established over the whole posterior distribution.

922 RMSE and AICc were calculated at the point of maximum likelihood (MAP). We report here the medians of those metrics, established across the

923 30 calibration re-samplings. The *CiHS* model results appear in bold characters, as displaying the highest PMW over validation data in all species.

924

Model class	Model name	PMW_{calib}	PMW_{valid}	$RMSE_{calib}$	$RMSE_{valid}$	$\Delta AICc_{calib}$	$\Delta AICc_{valid}$
threshold	Tt	0.00	0.00	14.7	15.0	226	89
threshold	TDLt	0.00	0.00	9.9	10.3	95	30
LADE (n calib= 210, n valid=90) heat sum	HS	0.00	0.01	8.2	8.7	36	8
chilling-influenced heat sum	**CiHS**	**1.00**	**0.94**	**7.5**	**8.1**	**0**	**0**
regression	MST	0.00	0.00	8.7	8.9	53	13
threshold	Tt	0.00	0.00	21.5	24.6	208	98
PISY threshold	TDLt	0.00	0.00	14.6	15.2	119	46
(n calib = 123, n valid = 52) heat sum	HS	0.00	0.00	11.4	11.2	63	18
chilling-influenced heat sum	**CiHS**	**1.00**	**1.00**	**8.4**	**9.3**	**0**	**0**

	regression	MST	0.00	0.00	15.6	15.6	133	49
PCAB (n calib = 236, n valid = 100)	threshold	Tt	0.00	0.00	16.8	17.2	378	151
	threshold	TDLt	0.00	0.00	12.4	12.6	221	92
	heat sum	HS	0.00	0.00	9.8	10.1	119	35
	chilling-influenced heat sum	**CiHS**	**1.00**	**1.00**	**7.5**	**7.9**	**0**	**0**
	regression	MST	0.00	0.00	11.5	11.6	154	62
PCMA (n calib = 206, n valid = 88)	threshold	Tt	0.00	0.00	13.1	13.2	334	139
	threshold	TDLt	0.00	0.00	7.3	7.3	116	45
	heat sum	HS	0.00	0.00	5.8	6.1	38	15
	chilling-influenced heat sum	**CiHS**	**1.00**	**0.67**	**5.2**	**5.6**	**0**	**0**
	regression	MST	0.00	0.33	6.7	6.9	32	1

925

926 **Table 4. Assessment of model bias on validation data**. We tested the model ability to produced unbiased predictions of bE from the validation

927 subsets at different scales, with two different methods (see Material and Methods 2.6 for details). The slopes and intercepts estimates are reported

928 with their 95%-confidence intervals between parentheses. Unbiased predictions are characterized by both slope= 1 and intercept=0. In Method 1,

929 we report the p-value of the Wald test (testing for unit slope and zero intercept as the null hypothesis). In Method 2, we identify biased

930 predictions when either the slope or intercept confidence intervals do not include one or zero, respectively. 'yes' / 'no' mark biased / unbiased

931 predictions.

bE data aggregation scale	Species	Method 1					Method 2		
		slope	intercept	F	P(>F)	Bias ?	slope	intercept	Bias ?
tree	LADE	1.04 (0.93, 1.15)	-6.2 (-23.0, 10.6)	0.41	0.66	**no**	0.67 (0.60, 0.74)	49.6 (38.4, 60.0)	yes
	PISY	1.02 (0.91, 1.12)	-4.2 (-16.5, 8.1)	2.57	0.08	**no**	0.79 (0.71, 0.87)	25.9 (16.3, 34.8)	yes
	PCAB	0.98 (0.92, 1.04)	2.5 (-5.4, 10.4)	0.34	0.71	**no**	0.88 (0.83, 0.93)	16.1 (8.9, 22.9)	yes
	PCMA	1.04 (0.94, 1.15)	-7.2 (-23.2, 8.7)	1.31	0.27	**no**	0.68 (0.61, 0.75)	49.2 (38.5, 59.2)	yes
site-year[*]	LADE	1.06 (0.90, 1.22)	-9.4 (-33.5, 14.6)	0.34	0.71	**no**	0.80 (0.68, 0.92)	30.6 (11.52, 47.6)	yes
	PISY	1.02 (0.85, 1.19)	-4.1 (-24.4, 16.2)	0.84	0.44	**no**	0.88 (0.74, 1.04)	15.4 (-3.1, 31.4)	**no**
	PCAB	0.99 (0.88, 1.10)	2.2 (-12.7, 17.1)	0.19	0.83	**no**	0.91 (0.81, 1.02)	11.8 (-2.6, 24.9)	**no**
	PCMA	1.01 (0.87, 1.16)	-3.1 (-25.1, 19.0)	1.83	0.18	**no**	0.91 (0.79, 1.05)	14.5 (-6.2, 33.3)	**no**
site[*]	LADE	1.13 (0.87, 1.40)	-19.3 (-58.8, 20.2)	0.72	0.51	**no**	0.82 (0.65, 1.04)	25.9 (-6.1, 52.3)	**no**
	PISY	1.03 (0.82, 1.23)	-6.0 (-31.3, 19.2)	0.97	0.4	**no**	0.92 (0.75, 1.13)	11.7 (-12.5, 31.8)	**no**
	PCAB	1.01 (0.83, 1.20)	-1.8 (-26.6, 23.1)	0.02	0.98	**no**	0.91 (0.76, 1.09)	11.47 (-13.0,	**no**

								32.2)	
	PCMA	1.27 (0.86, 1.68)	-42.0 (-102.1, 18.2)	3.55	0.11	**no**	0.75 (0.53, 1.03)	38.4 (-1.8, 70.2)	**no**
year anomaly[**]	LADE	1.02 (0.81, 1.23)	0 (-1.1, 1.1)	0.02	0.98	**no**	0.73 (0.59, 0.89)	0 (0, 0)	yes
	PISY	1.20 (0.67, 1.74)	0 (-2.0, 2.0)	0.3	0.74	**no**	0.43 (0.25, 0.64)	0 (0, 0)	yes
	PCAB	1.17 (1.00, 1.34)	0 (-1.1, 1.1)	2.02	0.14	**no**	0.69 (0.60, 0.80)	0 (0, 0)	yes
	PCMA	0.89 (0.74, 1.04)	0 (-0.8, 0.8)	1.06	0.36	**no**	1.02 (0.86, 1.21)	0 (0, 0)	**no**

932 * bE dates were simulated at the tree individual scale, and subsequently averaged at the site-year or site scale; ** bE dates were simulated at the tree individual

933 scale. For calculating annual anomalies, we subtracted the average bE date, established along the observation period, to bE data averaged at the site-year scale.

934

Figure captions

Figure 1. Location of the study sites.

Figure 2. Climate space at the observed date of bE. Each bE datum is placed in a climate

space defined by the day length at bE (x-axis) and the average temperature over the 15-day

interval preceding bE (y-axis).

Figure 3. Chilling-influenced heat sum (*CiHS*) model evaluation over validation data.

Predictions are reported at the tree scale (grey dots) and aggregated site-year scale (points,

colours according to the average January-June temperature of the site-year). The thick black

line is the least square regression line of predicted versus observed data. The one-to-one

relation appears as the thin grey line. *NSE*= Nash-Sutcliffe model efficiency; *slope*= slope of

the linear regression; *int*= intercept of the linear regression. The displayed statistics are

calculated for site-year aggregated data. See Table 3 for statistics on tree-scale data.

Figure 4. Posterior parameter distributions. Parameters are shown for the *CiHS* model,

which performed best over the validation data for each species. Grey lines represent each of

the 30 inference procedures, with the overall distribution appearing as coloured line. For each

parameter, the limits on the x-axis mark the bounds set to the uniform prior density. The mode

of the overall distribution appears for each parameter on the upper left-hand corner (e.g.

DL_{Cstart} = 12.7 hours for LADE). See Material and Methods for parameters description, and

Table S2 for parameter values at the mode of the merged 30 posterior distributions.

Figure 5. Variations of chilling and forcing accumulation time intervals along latitudinal

gradients. This figure displays the temporal interval of chilling accumulation (with the

starting date plotted as '*' and the ending date as 'o', linked by a straight line) and the starting

date of forcing (plotted as '△'). The colour of the symbols indicates the northernmost (blue)

or southernmost (red) latitude by species. For PCAB, we also illustrate an intermediate

situation (latitude = 54°N, grey symbols). Dashed black line represents vernal equinox;

continuous black line represents summer solstice.

Figure 6. Comparing observed and simulated interspecific differences in the date of bE.

For those site-years where two species of interest have been sampled simultaneously, we

plotted the observed and predicted between-species differences in bE dates (ΔbE, days). Each

964   single point represents one site-year. (a, b): compare the distribution of differences; (c, d):

965   compare observed and predicted differences for each site-year.

Supporting information

Additional supporting information may be found in the online version of this article.

Figure S1. Logistic models are precise in determining temperature thresholds for the beginning of xylem growth, but are not predictive.
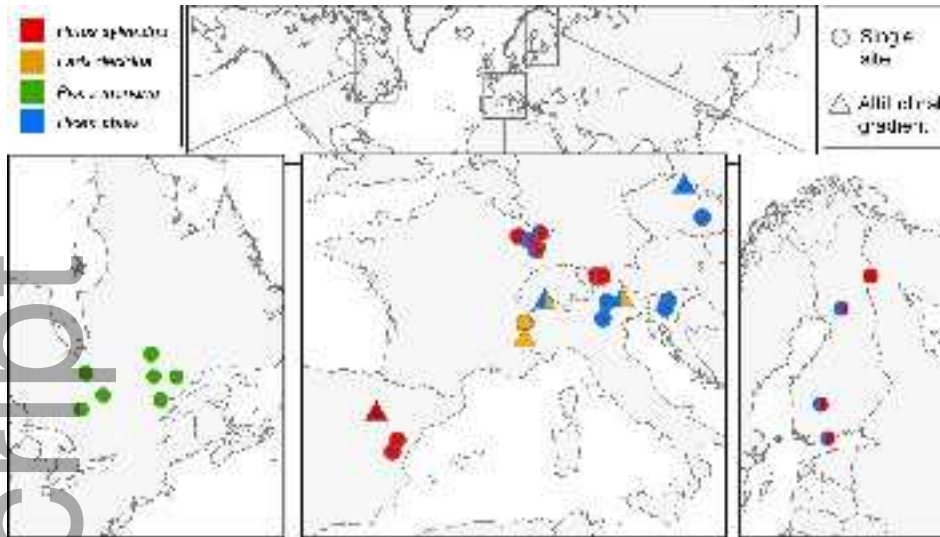
Figure S2. Model evaluation performance over validation data, aggregated per site.

Figure S3. Model evaluation performance over validation data, for annual anomalies.

Table S1. Study sites.

Table S2. Parameter values for the chilling-influenced heat sum (*CiHS*) model.

gcb_14539_f1.tif

gcb_14539_f2.eps

LADE

a

RMSE=5.2
NSE=0.63
slope=1.06
int=-9.44

PISY

b

RMSE=8.7
NSE=0.77
slope=1.02
int=-4.1

PCAB

c

RMSE=6.4
NSE=0.79
slope=0.99
int=2.17
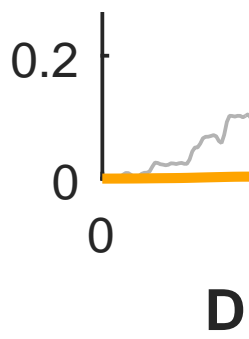
PCMA

d

RMSE=2.9
NSE=0.81
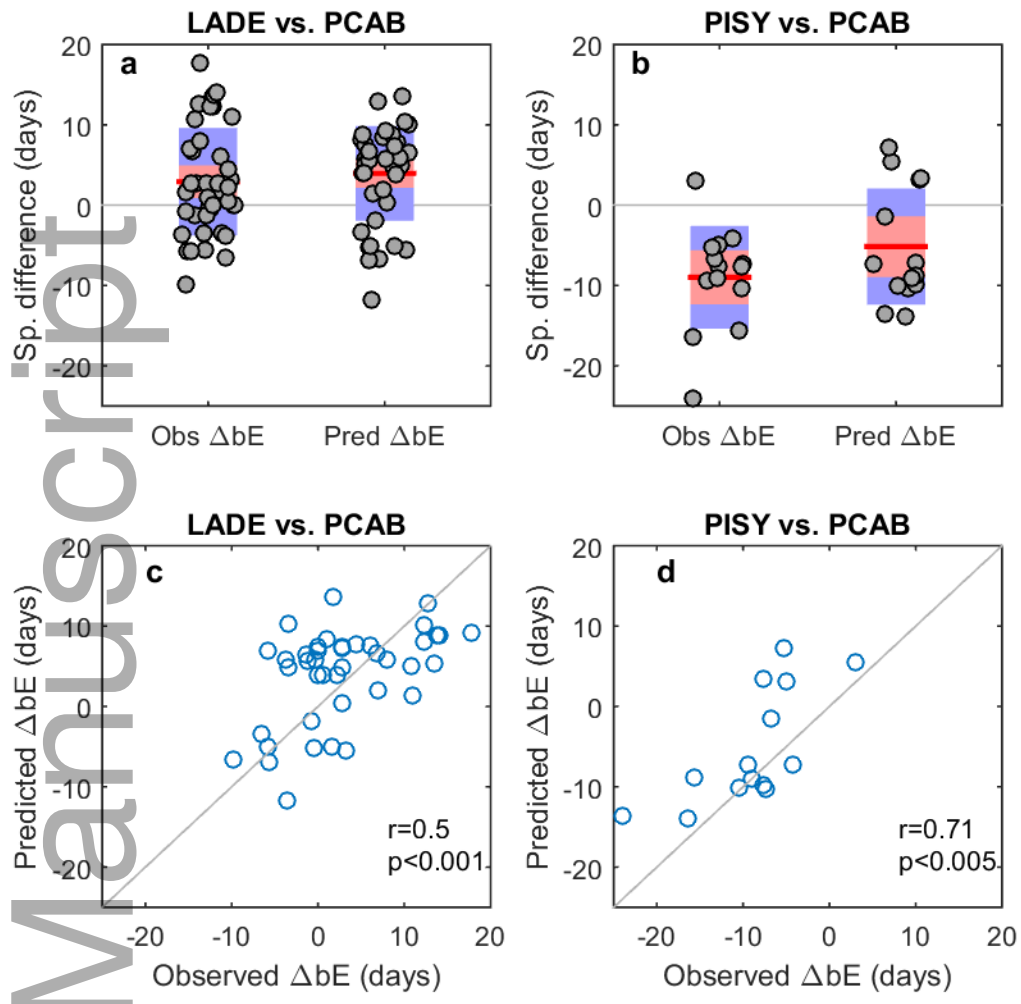slope=1.01
int=-3.06

Observed bE (DoY)

Predicted bE (DoY)
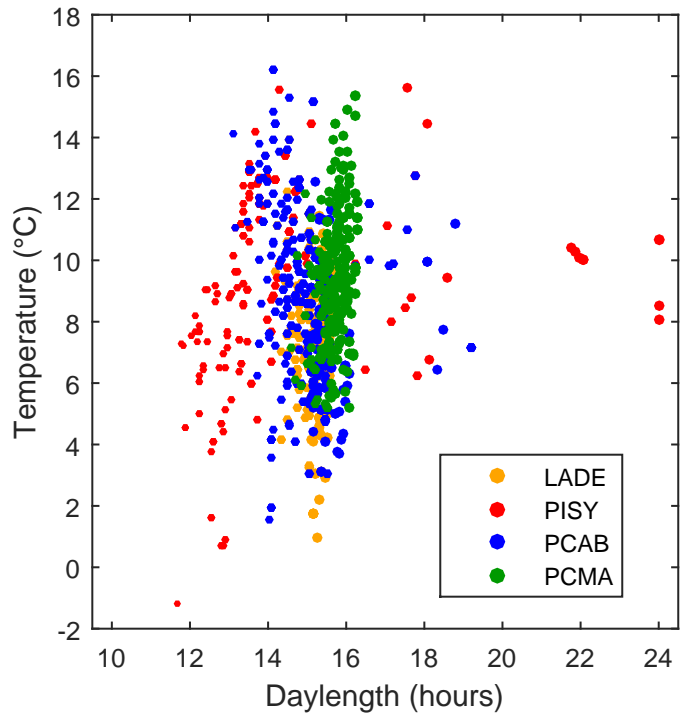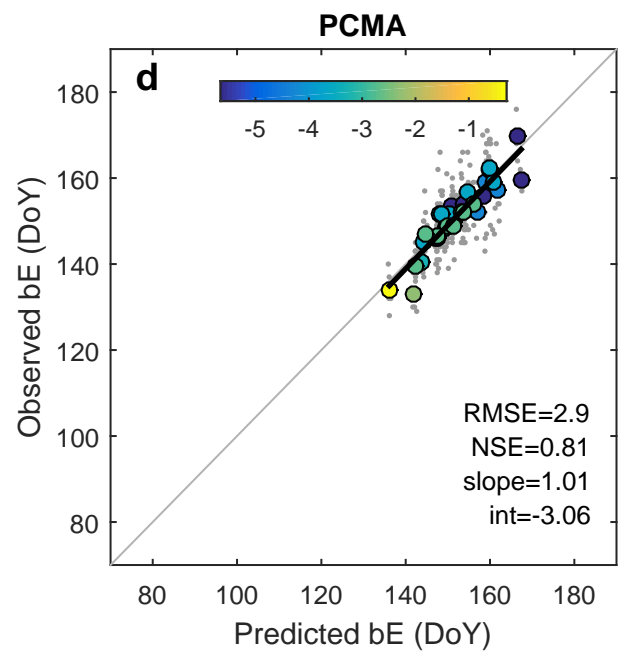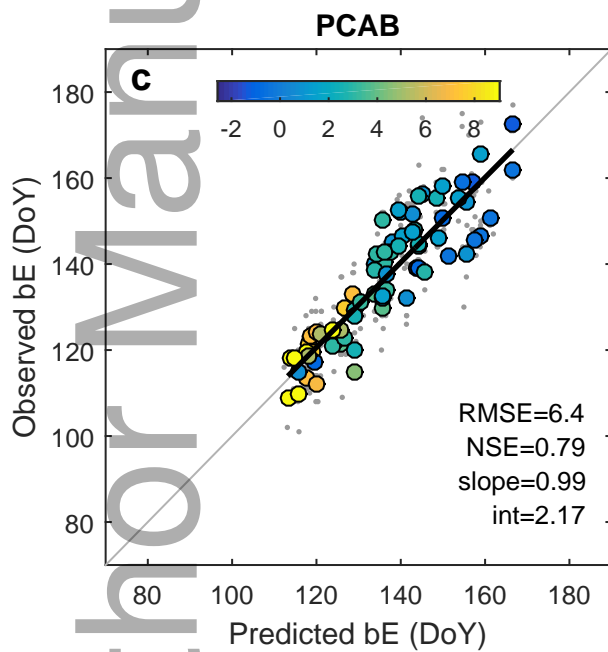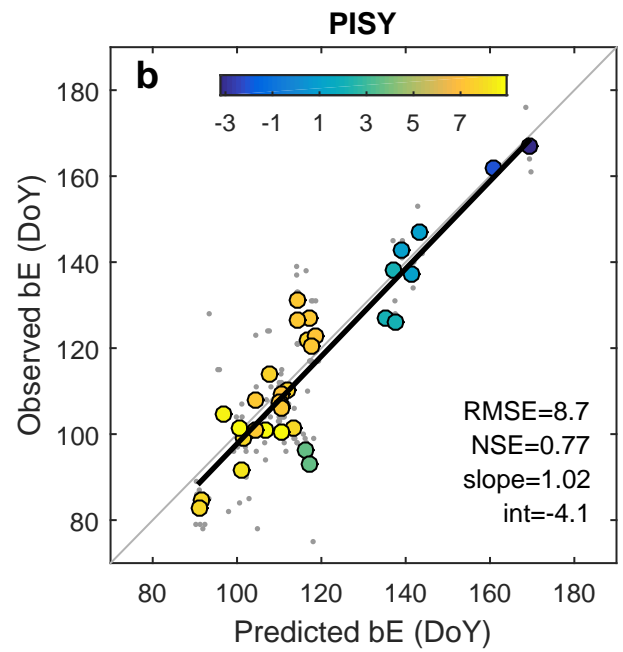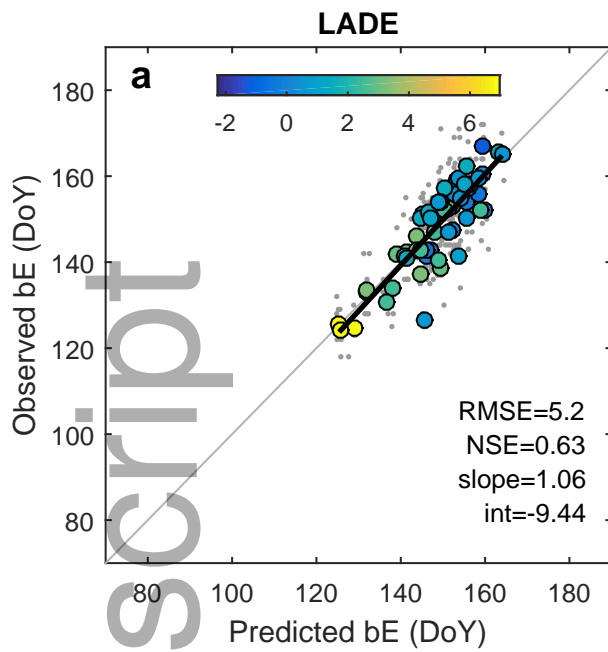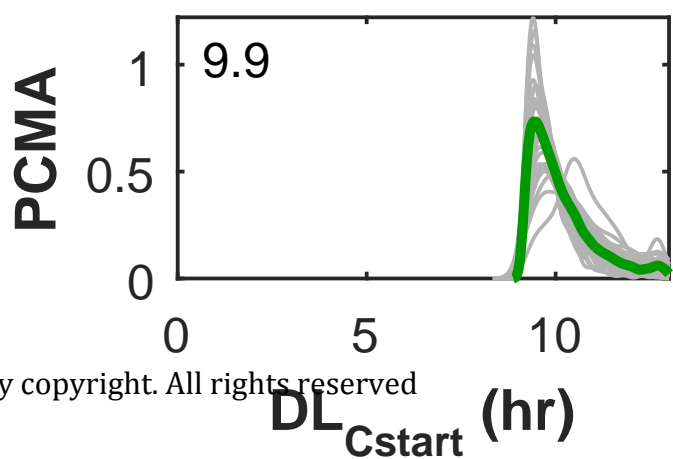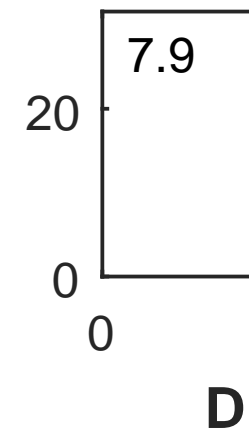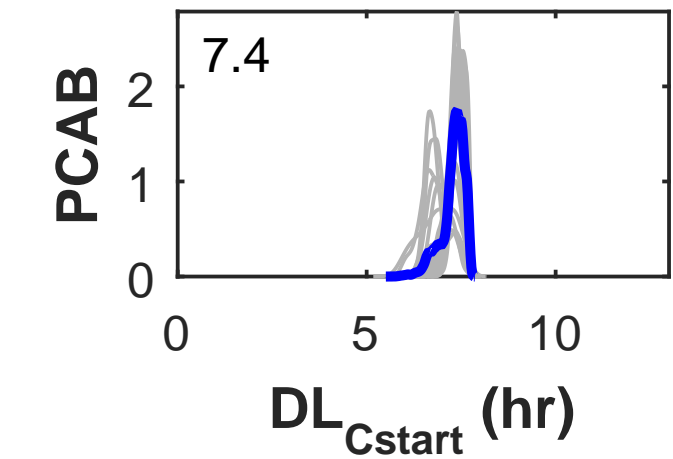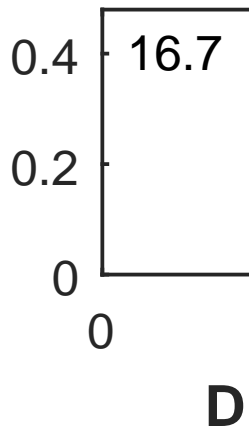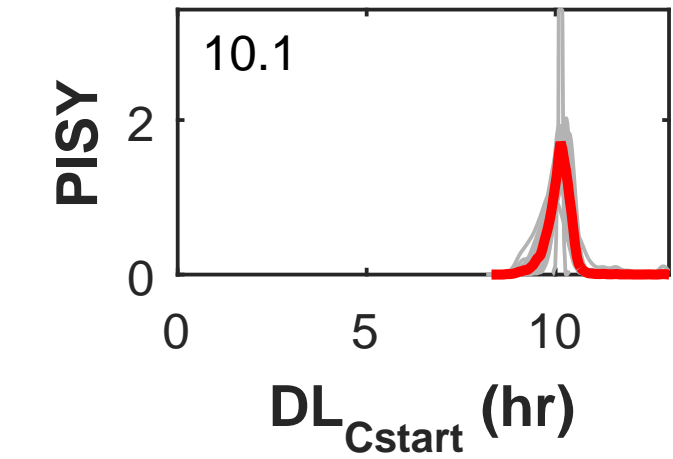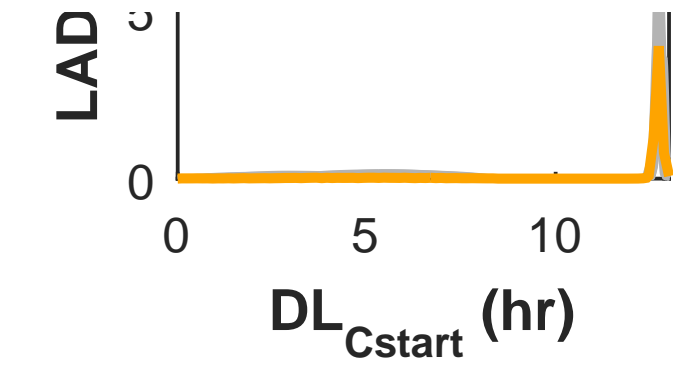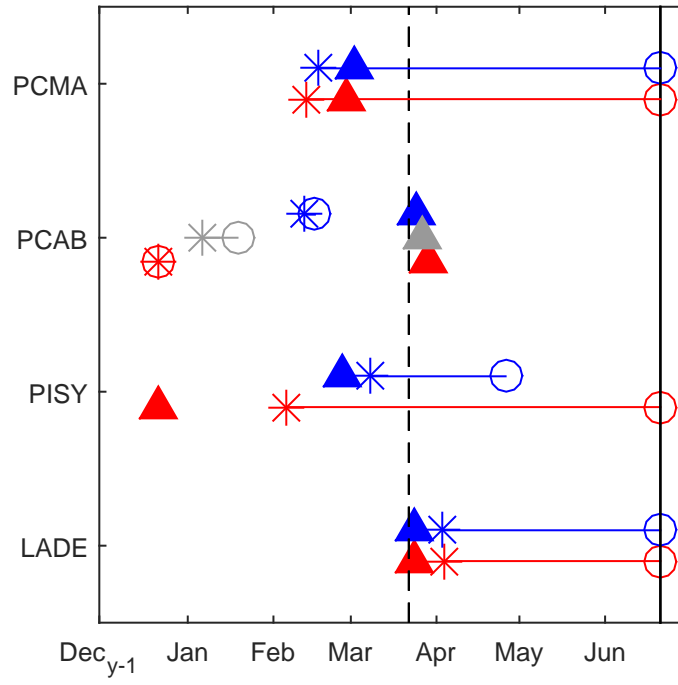
gcb_14539_f3.eps

gcb_14539_f5.eps

gcb_14539_f6.tif